DEPARTMENT OF DEFENCE
DEFENCE SCIENCE & TECHNOLOGY ORGANISATION
DSTO

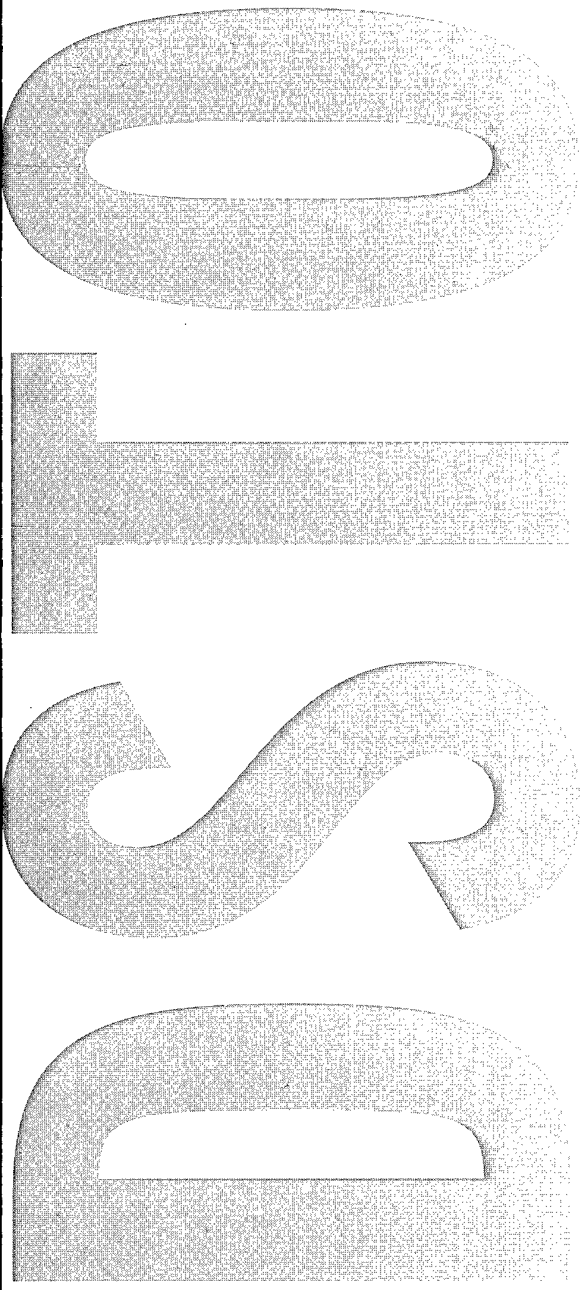

Ab Initio Calculation of Intermolecular Potential Parameters for Gaseous Decomposition Products of Energetic Materials

A. White, F.J. Zerilli and H.D. Jones

DSTO-TR-1016

Ab Initio Calculation of Intermolecular Potential Parameters for Gaseous Decomposition Products of Energetic Materials

A. White [a], *F.J. Zerilli* [b] *and H.D. Jones* [b]

[a] Weapons Systems Division
Aeronautical and Maritime Research Laboratory

[b] Energetic Materials Research and Technology Department
Naval Surface Warfare Center - Indian Head Division
Indian Head, MD 20640-5035, USA

DSTO-TR-1016

ABSTRACT

This document describes the results obtained using two methods for *ab initio* calculation of intermolecular potential parameters for gaseous decomposition products of energetic materials: a Multipole Expansion method, suitable for axially symmetric molecules, and a Monte Carlo method, which can be used to obtain temperature dependent average potential energy parameters for any molecule.

RELEASE LIMITATION

Approved for public release

DEPARTMENT OF DEFENCE
DEFENCE SCIENCE & TECHNOLOGY ORGANISATION
DSTO

Published by

DSTO Aeronautical and Maritime Research Laboratory
PO Box 4331
Melbourne Victoria 3001 Australia

Telephone: (03) 9626 7000
Fax: (03) 9626 7999

AR-011-531
August 2000

APPROVED FOR PUBLIC RELEASE

Ab Initio Calculation of Intermolecular Potential Parameters for Gaseous Decomposition Products of Energetic Materials

Executive Summary

The weapons systems of the Australian Defence Force rely on energetic materials for rocket and projectile propulsion (propellants) and terminal effects (explosives). In addition to research aimed at decreasing energetic material sensitivity for greater safety, improvements in performance are also being sought for increased range and thrust control in propellants and for enhanced terminal effects in explosives.

It is necessary to model the decomposition of energetic materials (combustion for propellants and detonation for explosives) in order to gain a predictive capability for the performance of existing and potential energetic materials which may be utilised in future weapons systems. The modelling of the decomposition processes involves sophisticated numerical models, which require equations of state describing properties of the decomposition products such as pressure, volume and internal energy. These decomposition products are largely gases, which in the high pressure, high temperature regime present during the combustion or detonation, are highly non-ideal. The non-ideal behaviour of gases is largely determined by the interactions between pairs of gas molecules which can be described as an intermolecular potential. Consequently, if we can obtain accurate estimates of the intermolecular potentials present, we can accurately model the decomposition of the energetic materials, leading to accurate estimates of their performance and decomposition behaviour.

Intermolecular potential parameters are generally obtained empirically by choosing them to be consistent with experimental results. However, if the intermolecular potentials can be obtained directly by computation, we can calculate their parameters independently of experiments, which can then be used to validate the results of experiments and also to give a predictive capability for areas where experiments have not, or can not, be conducted. *Ab initio* molecular orbital theory enables the calculation of molecular parameters, such as geometry and energy, using only approximations to the Schrödinger equation, without requiring any experimental data or assumptions from the system under study. The purpose of the current study was to attempt to obtain intermolecular potentials for gaseous products of energetic material decomposition for use in equations of state using only *ab initio* molecular orbital calculations[1]. It was found that these potentials can be calculated to a good degree of accuracy, giving valuable inputs for equations of state and allowing the subsequent calculation of the performance of energetic materials.

---

[1] The work presented in this document was commenced while Dr Alex White was on Long Term Attachment to the Naval Surface Warfare Center, Indian Head, Maryland and subsequently completed after his return to DSTO Salisbury.

Authors

A. White

Weapons Systems Division

Alex White is a Research Scientist in Propulsion Systems Technology group of Weapons Systems Division, DSTO. He obtained a Ph.D. in 1987 in physical inorganic chemistry studying ligand exchange processes in lanthanide and other complexes. He joined DSTO in 1988 and has since worked in several diverse areas including gun propellant service life, cost-benefit analysis of insensitive munitions, weapons effectiveness studies and computational chemistry. He recently returned from a long-term attachment to the Naval Surface Warfare Center, Indian Head, MD in the United States of America where this work was commenced.

F.J. Zerilli

Energetic Materials Research and Technology Department
Naval Surface Warfare Center Indian Head Division
Indian Head, MD 20640-5035, USA

Frank J. Zerilli is a Research Scientist in the Energetic Materials Research and Technology Department of the Naval Surface Warfare Center, Indian Head, Maryland, USA. He received his Ph.D. in 1969 in theoretical physics studying the physics of black holes. After several years of teaching and research at universities, he joined NSWC in 1979 where he has done research on the equation of state and strength of materials, both energetic and non-energetic.

H.D. Jones

Energetic Materials Research and Technology Department
Naval Surface Warfare Center Indian Head Division
Indian Head, MD 20640-5035, USA

Contents

1. Introduction

The weapons systems of the Australian Defence Force rely on energetic materials for rocket and projectile propulsion (propellants) and terminal effects (explosives). In addition to research aimed at decreasing energetic material sensitivity for greater safety, improvements in performance are also being sought for increased range and thrust control in propellants and for enhanced terminal effects in explosives.

It is necessary to model the decomposition of energetic materials (combustion for propellants and detonation for explosives) in order to gain a predictive capability for the performance of existing and potential energetic materials which may be utilised in future weapons systems. This modelling involves sophisticated numerical models of the decomposition processes [1], which in turn require equations of state describing properties of the decomposition products such as pressure, volume and temperature. These decomposition products are largely gases, which in the high pressure, high temperature regime present during combustion or detonation, are highly non-ideal. The non-ideal behaviour of gases is largely determined by the interactions between pairs of gas molecules which can be described by an intermolecular potential. Consequently, if we can obtain accurate estimates of the intermolecular potentials present between gaseous products of energetic material decomposition, we can realistically model the decomposition processes which occur in energetic materials to obtain accurate estimates of their performance and decomposition behaviour.

Intermolecular potential parameters are generally obtained empirically by choosing them to be consistent with experimental results. However, if intermolecular potential parameters can be obtained directly by computation independently of experiments, they can then be used to validate the results of experiments and also to give a predictive capability for areas where experiments have not, or can not, be conducted.

Ab initio molecular orbital theory enables the calculation of molecular parameters such as geometry and energy, using only approximations to the Schrödinger equation, without requiring any experimental data or assumptions from the system under study. The purpose of the current study was to attempt to obtain intermolecular potentials for gaseous products of energetic material decomposition for use in equations of state using only *ab initio* molecular orbital calculations. For simplicity, only axially symmetric (linear) molecules will be considered here. A more complex example (H_2O) will be addressed in a subsequent publication [2].

This work was commenced while Dr Alex White was on Long Term Attachment to the Naval Surface Warfare Center, Indian Head Division, Indian Head, Maryland, United States of America.

2. Theory

2.1 Energetic Materials Decomposition

2.1.1 Shock in an explosive without reaction

A shock travelling through a material such as a solid explosive constitutes a discontinuous (or approximately so) jump in the pressure and particle velocity. A solid explosive at atmospheric pressure (P_0) occupies a specific volume V_0 ($V_0 = 1/\rho_0$ where ρ_0 is the initial density of the explosive), has specific internal energy E_0 and initial particle velocity U_0. If a shock wave passes through the material with velocity D but does not heat the material sufficiently to initiate reaction, the shocked material will be at a new specific volume V, pressure P and specific internal energy E. The new particle velocity is U. Assuming steady-state conditions, laws of conservation of energy, momentum and mass hold across the shock (collectively called the "Rankine-Hugoniot conditions") [1, 3, 4, 5]:

- conservation of energy:

$$E - E_0 = \frac{1}{2}(P + P_0)(V_0 - V) \tag{1}$$

- conservation of momentum:

$$(D - U_0)^2 = V_0^2 \frac{(P - P_0)}{(V_0 - V)} \quad \text{or} \quad \rho_0^2 (D - U_0)^2 = \frac{(P - P_0)}{(V_0 - V)} \tag{2}$$

- conservation of mass:

$$\frac{V}{V_0} = \frac{(D - U)}{(D - U_0)} \tag{3}$$

Substituting an equation of state (see Section 2.2 below) describing E (or temperature, T) in terms of V and P into equation (1) gives a curve in the V-P plane passing through the initial state (V_0, P_0) called the shock Hugoniot (Figure 1). It is the locus of all possible states possible for the explosive produced by shocks of varying strength from that initial state (again assuming no reaction). Equation (2) defines a line plotted in the V-P plane called the Rayleigh line joining the initial state (V_0, P_0) and the shocked state (V, P). The slope of the Rayleigh line through (V, P) and (V_0, P_0) is $-\rho_0(D-U_0)^2$, and so is proportional to the square of the shock velocity D. The Rayleigh line represents the jump condition from the unshocked to the shocked state [4] and, knowing (V, P) and (V_0, P_0), can be used to obtain the shock velocity D or alternatively, knowing D and (V_0, P_0), can be used to calculate the shocked state (V, P). Equation (3) can then be used to obtain U, the particle velocity behind the shock.

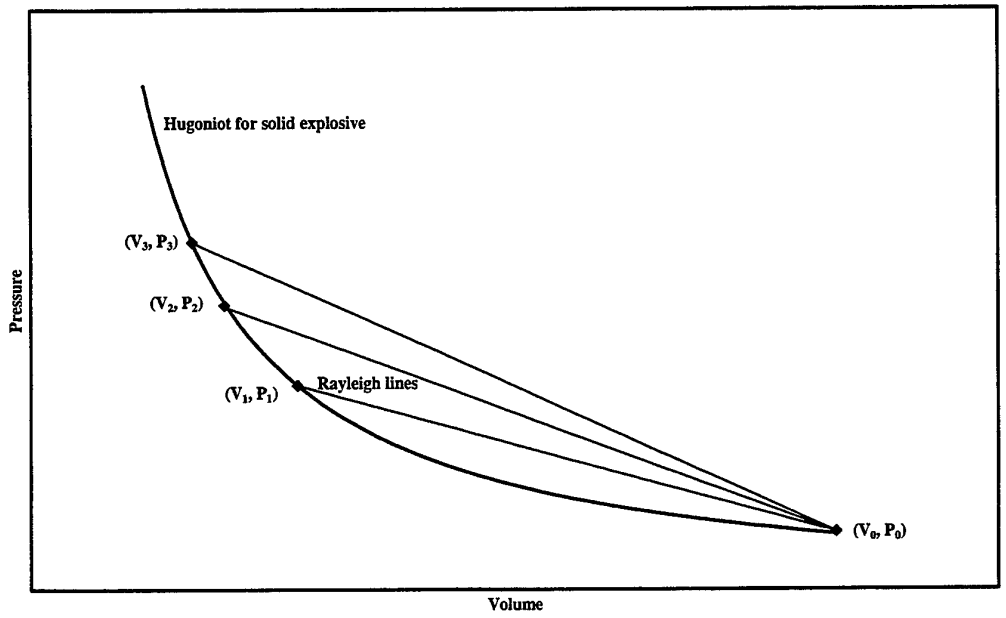

Figure 1: Shock Hugoniot curve and Rayleigh lines for a solid explosive (without reaction)

2.1.2 Shock in an explosive with reaction (detonation)

If the shock in the explosive is sufficiently strong, it may heat the explosive sufficiently to cause a reaction, in which case a reaction zone will form behind the shock front. There will be a family of reaction Hugoniots, one for each reaction coordinate extending through the reaction zone [5]. The final reaction Hugoniot is the "detonation Hugoniot" or the "Hugoniot of the reaction products" (Figure 2). It is displaced from the shock Hugoniot for the unreacted explosive by the heat of reaction ($q = -\Delta H$) and so does not pass through the initial point (V_0, P_0). Behind the reaction zone the gaseous detonation products are free to expand through a rarefaction ("Taylor") wave. The products expand along an isentrope which is closely approximated by the detonation Hugoniot so that it can be considered that the products "unload" via a family of Rayleigh lines in infinitesimal steps down the detonation Hugoniot [4]. Thus the slope of the detonation Hugoniot in the shocked state (ie, the slope of the first infinitesimal unloading Rayleigh line) is proportional to the square of the velocity of the rear of the reaction zone (or, equivalently, the front of the rarefaction wave).

The conservation rules given above still apply, if we assume that the steady-state conditions include the reaction zone, ie that the rear of the reaction zone moves at the same speed as the shock front and V and P are now the specific volume and pressure of the reaction products rather than the solid explosive. Again, an equation of state for the reaction products describing E (or T) in terms of V and P is required to obtain the Hugoniot for the reaction products.

Three possible situations can be imagined regarding the relative position of a particular Rayleigh line corresponding to a shock state in the solid explosive and the detonation Hugoniot as shown in Figure 2:

(a) the Rayleigh line may pass below the detonation Hugoniot (as in (V_0, P_0) – (V_1,P_1)). The shock velocity is insufficient to cause reaction to detonation (ie, there cannot be a steady-state detonation, only a deflagration).

(b) the Rayleigh line may pass through the detonation Hugoniot with two points of intersection (as in (V_0, P_0) – (V_3,P_3)). At the upper intersection point (V_4, P_4), the rear of the reaction zone would have a greater velocity (slope of the Hugoniot) than the shock front (slope of the Rayleigh line) and would overtake it, in violation of the steady-state assumption. At the lower point (V_5, P_5), the rear of the reaction zone would have a lower velocity than the shock front and would increasingly lag behind it, again violating the steady-state assumption.

(c) the Rayleigh line and the detonation Hugoniot may touch tangentially (as in (V_0, P_0) – (V_2,P_2)) at the so-called Chapman-Jouguet (CJ) point. At this point, the velocities of the reaction zone, reaction products and the shock front in the solid explosive are all the same (D_{CJ}), and so this is the only point on the detonation Hugoniot where a steady-state detonation can occur [4].

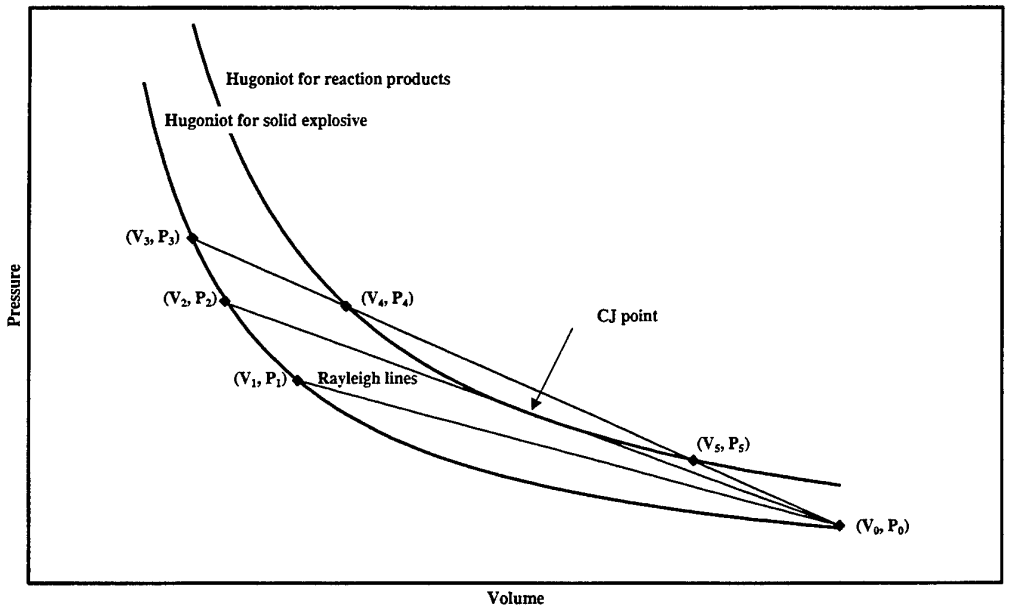

Figure 2: Hugoniot curves for solid explosive and reaction products and Rayleigh lines

In summary, a steady-state shock front passing through an explosive with velocity D_{CJ} compresses the solid explosive to a specific volume V_2, raising the pressure to P_2 (and raising the temperature to a value determined by the equation of state for the solid explosive), thus initiating chemical reaction. A reaction zone follows the shock front, and on completion of the reaction, the reaction products are at the volume and pressure at the CJ point on the detonation Hugoniot. These products then expand in a

rarefaction ("Taylor") wave behind the reaction zone. In a steady-state detonation, the shock front, reaction zone and front of the rarefaction wave are moving at the same velocity (D_{CJ}).

Thus, if the elemental composition, density and heat of formation of a solid explosive are known, an equation of state relating E, P and V of the reaction products can be used in conjunction with the conservation relationships described above to calculate C-J detonation parameters of an explosive such as equilibrium detonation product composition and pressure and temperature. These calculations are described in detail in [1] using the BKW computer code.

2.1.3 Combustion of propellants

Equations of state for mixtures of gases and solid decomposition products by definition do not depend on the path taken to reach that state. Consequently, in addition to detonation properties of explosives, equation of states are equally applicable to prediction of propellant performance.

2.2 Equations of State

State functions are functions which only depend on the current state of the system, not on it's history. Examples include pressure, temperature and volume. State functions of a particular system are related by an equation of state (EOS). As described above, an EOS relating internal energy E, pressure P and volume V is required to substitute into the conservation equations given above to solve them and obtain the relevant Hugoniots and detonation or combustion properties.

The relationship of internal energy to volume is given by [7]:

$$\left(\frac{\partial E}{\partial V}\right)_T = T\left(\frac{\partial P}{\partial T}\right)_V - P$$

Integrating this expression at constant temperature and fixed composition gives the energy of a system at temperature and volume (T, V) in terms of its energy at temperature T and reference volume V* [1]:

$$E(T,V) = E(T,V^*) + \int_{V^*}^{V}\left[T\left(\frac{\partial P}{\partial T}\right)_V - P\right]dV$$

where $(\partial P/\partial T)_V$ is obtained from the EOS relating P, V and T (see below).

2.2.1 *The ideal gas law*

One of the simplest and best known equations of state is the "ideal gas law" which relates the pressure (P), volume (V), temperature (T) and amount of gas (n) using the universal gas constant (R):

$$PV = nRT$$

or if we define molar volume as $V_m=V/n$:

$$PV_m = RT$$

For an ideal gas, $(\partial P/\partial T)_V = nR/V$, so that $(\partial E/\partial V)_T = nRT/V - P = 0$, giving $(\partial E/\partial T)_P = C_V = (\partial E/\partial T)_V$ where Cv is the heat capacity of the gas at constant volume. Thus, for an ideal gas, the internal energy is a simple function of T, and does not depend on V or P.

The ideal gas law assumes that there are no forces present between the molecules of the gas and that the gas molecules occupy no volume. It is only applicable where the forces between molecules in the gas are negligible compared with the thermal effects of the gas, ie at low pressures. As the pressure increases, interactions between the gas molecules become significant. At moderate pressures, the forces between the gas molecules tend to be more attractive than in the ideal gas case (where there are no forces between the molecules). This is due to van der Waals forces which arise from electron correlation between molecules[1]. At very high pressures, the molecules are forced together so closely that there is non-bonded overlap between the electron clouds which in itself is repulsive, but also results in incomplete shielding of the nuclei resulting in a strong electrostatic repulsion (short range). Consequently, real gases tend to be easier to compress than ideal at moderate pressures due to long range attractive forces but harder to compress at high pressures due to short range repulsive forces [7]. Equations of state for real gases need to be more complex than the ideal gas law.

2.2.2 *The van der Waals equation of state*

Various improvements on the ideal gas law have been proposed for real gases which exhibit non-ideal behaviour. For example, if we take account of:

(a) the fact that the molecules in a gas take up volume, so that when a gas is compressed, the molecules only have a volume of *V-nb* to move into (where b is the volume occupied by one mole of molecules) and

[1] This can be thought of in a classical (non-quantum mechanical) sense in the following way: Due to electron movement, the electric field arising from the electrons in a molecule at any instant is not completely uniform, ie., there is a net dipole. This instantaneous dipole induces an opposite electric dipole in nearby molecules causing a net attraction. See [6] for more details.

(b) the attractive force between molecules is proportional to the density of molecules and so reduces the observed pressure proportionally to the density (pressure reduced by an^2/V^2),

the "van der Waals" EOS can be obtained [7]:

$$P = \frac{nRT}{(V - nb)} - \frac{an^2}{V^2}$$

or substituting $V_m = V/n$:

$$P = \frac{RT}{(V_m - b)} - \frac{a}{V_m^2}$$

Although the van der Waals EOS allows better approximation to real systems through the use of the two coefficients, a and b, it fails at high pressures and densities because it assumes that the molecules have a well-defined diameter and does not take into account the actual intermolecular forces which lead to the apparent molecular diameter.

2.2.3 *The virial equation of state*

The van der Waals EOS is a particular case of the virial EOS. In general, the virial EOS uses a power series to model the behaviour of non-ideal gases:

$$\frac{PV_m}{RT} = 1 + \frac{B(T)}{V_m} + \frac{C(T)}{V_m^2} + \cdots$$

where B(T) is the second virial coefficient, C(T) is the third, etc. It can be seen that if the coefficients are all zero, this expression reduces to the ideal gas equation. It follows then that the virial coefficients must arise from the effects of the intermolecular forces in a real gas. It can be shown that B(T) depends on the intermolecular potential (V(r)) between pairs of molecules[2] [7]:

$$B(T) = 2\pi N_A \int_0^\infty \left(1 - e^{-V(r)/kT}\right) r^2 dr$$

where N_A is Avogadro's constant, k is Boltzmann's constant and r is the intermolecular distance. Consequently, if we know the form of the intermolecular pair potential V(r) for a particular gas, we can evaluate B(T) and obtain the virial EOS (at least approximately to the second order) for that gas.

[2] The third virial coefficient C(T) depends on interactions between groups of three molecules and so on.

2.2.4 *The Becker-Kistiakowsky-Wilson (BKW) equation of state*

The Becker-Kistiakowsky-Wilson (BKW) EOS is based on a repulsive potential applied to the virial EOS [1]. If terms higher than third order are neglected, the virial EOS becomes:

$$\frac{PV_m}{RT} = 1 + \frac{B(T)}{V_m} + \frac{C(T)}{V_m^2}$$

by setting $x = B(T)/V_m$ this can be rewritten as:

$$\frac{PV_m}{RT} = 1 + x + \beta x^2$$

or approximately:

$$\frac{PV_m}{RT} = 1 + xe^{\beta x}$$

If a repulsive potential of the form $U=A/r^n$ is used, then:

$$B(T) = \frac{K}{(T+\Theta)^\alpha} \quad \text{or} \quad x = \frac{K}{V_m(T+\Theta)^\alpha}$$

where $\alpha = 3/n$ and $K \propto A^{3/n}$ (the constant Θ is introduced to prevent the pressure tending to infinity as the temperature approaches zero. It is given an arbitrary value of 400 K [1]). Thus the BKW EOS for a pure gas is [1]:

$$\frac{PV_m}{RT} = 1 + xe^{\beta x} \quad \text{where} \quad x = \frac{K}{V_m(T+\Theta)^\alpha}$$

For a mixture of detonation products, the more common form of the BKW EOS is [1]:

$$\frac{PV_m}{RT} = 1 + xe^{\beta x} \quad \text{where} \quad x = \kappa \frac{\sum X_i k_i}{V_m(T+\Theta)^\alpha}$$

where X_i and k_i are respectively the mole fractions and covolumes[3] of the detonation products and α, β and κ are EOS constants. α is generally around 0.5 and β and κ can

[3] the geometrical covolume is defined as the volume occupied by a molecule rotating about its centre of mass x 10.46 [1]. This represents the repulsive potential of each detonation product in a similar way to b in the van der Waals equation of state. Although a covolume can be calculated from the molecular dimensions, the best method of evaluating the covolume of a product molecule is from the experimental shock Hugoniot [1].

be obtained by iteratively fitting experimental detonation data. Generally, two sets of parameters are used, one based on RDX for most explosives and one based on TNT for explosives with large amounts of solid carbon in the detonation products [1].

Mader [1] describes in detail the application of the BKW computer code to predict the performance of explosive mixtures and propellants using the BKW EOS [8] for gaseous detonation products and the Cowan EOS [9] for solid detonation products.

2.2.5 *The Jones-Zerilli equation of state*

The EOS applicable to the work described in this document is detailed in [10]. It is based on the formalism of Weeks, Chandler and Anderson [11] that repulsive intermolecular forces dominate the characteristics of the fluid phase. It is assumed that the intermolecular interaction is spherically symmetric and can be expressed in the form [10]:

$$V(r) = u_0(r) + w(r)$$

where $u_0(r)$ is the reference repulsive potential:

$$u_0(r) = \begin{cases} V(r) - V(r_c) & r \le r_c \\ 0 & r > r_c \end{cases}$$

and w(r) is an attractive perturbation:

$$w(r) = \begin{cases} V(r_c) & r \le r_c \\ V(r) & r > r_c \end{cases}$$

where r is the intermolecular distance and V(r) is the exp-6 potential with the temperature dependent well depth as described in Section 2.3 below. Thus the potential is arbitrarily taken to be divided at the intermolecular distance r_c[4]. Weeks, Chandler and Andersen [11] took the breakpoint r_c to be the intermolecular distance at the maximum well depth (r^* below), however Ree [20] demonstrated that by taking r_c to be a variational parameter, the method could be extended to the high-density domain of interest in studies of detonation phenomena.

[4] The symbol λ is generally used for the breakpoint of the potential, however the symbol r_c has been used here to avoid confusion as the symbol λ is used extensively below to refer to a different parameter.

2.3 Intermolecular Potentials

Historically, the Lennard-Jones (LJ) potential [12, 13] has been widely used to model intermolecular interactions. The LJ intermolecular potential ϕ has a twelfth power repulsive term and a sixth power attractive term:

$$\phi = 4\varepsilon\left[\left(\frac{\sigma}{r}\right)^{12} - \left(\frac{\sigma}{r}\right)^{6}\right]$$

where r is the intermolecular separation, σ is the intermolecular distance where the potential is zero and ε is the potential well depth. The form of the LJ potential is shown in Figure 3 along with the parameters just described. The attractive tail arises from van der Waals interaction due to electron correlations while the strongly repulsive core is due to nonbonded overlap between electron clouds [14, 6].

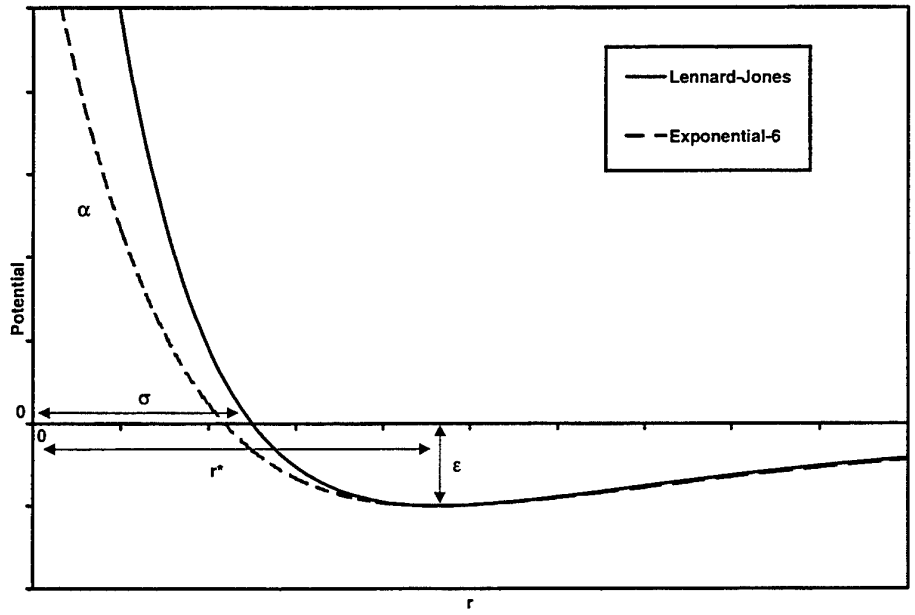

Figure 3: The form of the Lennard-Jones (LJ) and the exponential-6 (exp-6) potentials.

However, the repulsive term in the LJ potential is known to be much too hard (ie, the repulsive core is too steep) at small intermolecular distances. A more realistic potential which agrees with molecular beam scattering data and gives the correct functional form at small intermolecular separations is the exponential-6 (exp-6) potential [15]:

$$\phi = \frac{\varepsilon}{(\alpha - 6)}\left[6e^{\alpha\left(1-\frac{r}{r^*}\right)} - \alpha\left(\frac{r^*}{r}\right)^6\right]$$

where ϕ is again the potential at intermolecular separation r, ε is again the potential well depth, r^* is now the intermolecular distance where the potential is a minimum (ie, where $\phi = -\varepsilon$) and α is a "steepness factor". The form of the LJ potential is shown in Figure 3 along with the parameters appropriate to this curve. It can be seen that the repulsive part of the curve is indeed "softer" than that of the LJ potential (the steepness factor for this curve has been scaled so that the attractive terms of the two curves are identical). In this work, the exp-6 potential was used exclusively.

In addition, the well depth ε is made temperature dependent via the expression [16]:

$$\varepsilon = \varepsilon_0\left(1 + \frac{\lambda}{T}\right)$$

to allow for multipole interactions which increase as the temperature decreases. This effect should only be important where the molecules have strong multipole interactions and where they do not have dipoles, λ is often assumed to be zero. The *ab initio* techniques described here allow the calculation of these parameters with no assumptions about the system under study. Consequently, they afford a method of checking if this assumption is valid.

3. Techniques

3.1 Introduction

As stated before, the object of this work was to use *ab initio* quantum chemical methods to obtain intermolecular potential parameters for use in equations of state for the products of energetic material decomposition. The intermolecular potential is the potential between two molecules and as seen in Section 2.3, varies with the intermolecular distance r. For real molecules which are not spherically symmetric, the intermolecular potential also varies in a complex fashion with the relative orientation of the two molecules. This is generally overcome by specifying a "spherically symmetric" potential, averaged over all possible relative molecular orientations for each intermolecular distance.

As described in Sections 3.5 and 3.6 below, two different techniques (the "Monte Carlo" (MC) and the "Multipole Expansion" (ME) techniques) were developed to obtain spherically symmetric intermolecular potentials and their associated parameters. Both techniques use *ab initio* methods to obtain the intermolecular potential between two molecules with various relative molecular orientations at several intermolecular distances. The methods differ in that while the MC method averages

many randomly generated orientations at each intermolecular distance, the ME method averages several specifically selected orientations by solving the set of equations giving the radial dependence of the potential.

Consequently, as discussed in more detail below, the general sequence followed to obtain the exp-6 potential parameters for the intermolecular potentials between two molecules was as follows:

1. Choose a suitable *ab initio* method to be used for the system of interest.
2. Obtain an optimised geometry for each molecule in isolation, giving equilibrium internal bond lengths and angles and a reference molecular energy. The internal geometry is fixed using these bond lengths and angles to make the molecules rigid.
3. For the two molecule system with a particular intermolecular separation, conduct *ab initio* calculations to obtain the energy of the system for several selected (ME method) or many randomly generated (MC method) molecular orientations. The intermolecular potential is this energy minus the reference energy of the two molecules in isolation (ie, at infinite distance).
4. Obtain the spherically symmetric potential at that intermolecular distance by averaging these intermolecular potentials using the MC or ME method as appropriate as described below.
5. Repeat steps 3 and 4 for several intermolecular separations over a sufficient range of the intermolecular potential.
6. Fit the data using the exp-6 potential curve to obtain the potential parameters.

3.2 *Ab initio* methods

A commercial computer program (Gaussian 98 [17]) was used to carry out the *ab initio* calculations of molecular geometry and energies. *Ab initio* methods are discussed in depth in [18]. For the purpose of this study, it is sufficient to note that a particular *ab initio* method is defined by two components, a theoretical method and a basis set.

The theoretical method generally specifies the level of electron correlation considered. In general, the greater the level of electron correlation considered, the more accurate the results, however at a cost in the use of computer resources (RAM, hard disk space and computation time). The Møller-Plesset perturbation method [19] was used in this study. For the ME method, the perturbation is taken to the fourth order (MP4) whereas for the MC method the perturbation was only taken to the second order (MP2). Although the latter is less accurate, it was necessary to use it for the large number of calculations required in the MC method.

The basis set gives a mathematical description of the orbitals used to calculate the total electronic wavefunction of the system. Again, the larger the basis set, the more accurate the results, but the greater the use of computer resources. For the MC method, a 6-311^{++}G(d,p) basis set was used. The "G" indicates that gaussian type orbitals are used. The "6-311" indicates an inner shell atomic orbital composed of six primitive gaussian functions and a valence shell composed of three sizes of basis function for

each valence orbital. These basis functions are composed of three, one and one primitive gaussian functions respectively. The "++" indicates the addition of diffuse functions (larger orbitals) to both hydrogen and heavy atoms, allowing for electron density at distances far from the nucleus. In the study of intermolecular potentials, these interactions are likely to be important. The (d,p) indicates that d-orbital type polarisation functions are added to heavy atoms while p-orbital type polarisation functions are added to hydrogen atoms. These polarisation functions allow the orbitals to change shape to allow for non-uniform displacement of charge from the nucleus, increasing the accuracy of the calculation over calculations only permitted to use the functions available from the filled orbitals. For example, a carbon atom may have d polarisation functions added, allowing a degree of "mixing-in" of the higher d orbitals to allow for non-uniform charge distribution in bonded atoms. For the ME method, which requires fewer calculations than the MC method, a larger basis set could be used, adding more polarisation functions, giving a 6-311++G(3df, 2pd) basis set.

The computer resources required for *ab initio* calculations also increase rapidly with the size of the system (number of atoms) under consideration. Thus there is always a compromise between the accuracy of the result and the computer resources and time available.

3.3 Molecular geometry optimisation

For both techniques, the first step is to optimise the bond lengths and angles for one molecule in isolation at the level of the subsequent calculation (Table 1). This is done by allowing the bond lengths and angles to change until a minimum in the molecular energy is found. The reference energy for the two molecule system is taken as twice this energy[5].

Table 1: Optimised Molecular Parameters

Method	Theoretical Method/Basis Set	Species	Bond Length (Å)	Energy (hartrees)
MC	MP2/6-311++G(d,p)	HF	0.916600	-100.27889234382
		H_2	0.738400	-1.1603010878136
		N_2	1.120264	-109.30155631903
		CO_2	1.169954	-188.20655793738
		CO	1.139923	-113.07816919596
ME	MP4/6-311++G(3df,2pd)	HF	0.917878	-100.34236767
		H_2	0.741210	-1.1717385902
		N_2	1.113093	-109.37982637
		CO_2	1.172760	-188.34271091
		CO	1.142857	-113.16255765

[5] Alternatively, the reference energy may be taken as the total energy of two molecules at effectively infinite separation. As expected, these values are, for practical purposes, identical. However, this can only be said of methods which are "size-consistent", ie, do not depend on the number of orbitals in the system. MP methods are size-consistent.

3.4 Specifying molecular orientation

We need to specify the orientation of two molecules relative to one another so that we may calculate the intermolecular potential for that particular orientation and then average these potentials for several orientations using either the Monte Carlo method (described in Section 3.5 below) or the Multipole Expansion method (described in Section 3.6).

We assume that the molecules under study are rigid bodies, ie that the bond lengths are fixed at the bond length of minimum molecular energy for the individual molecules obtained in Section 3.1. For each molecule, a set of Cartesian coordinate axes can be assigned with the origin at the centre of mass (CoM) of the molecule. The relative orientation of any two molecules can then be defined relative to an imaginary line joining the centres of mass of the two molecules. In general, this is done by specifying three angles ("Euler angles") for each molecule. However, symmetry considerations may reduce the number of angles that it is necessary to specify. For two axially symmetric molecules (ie, molecules which have a $C_{\infty v}$ axis), only three angles need to be specified as shown in Figure 4 [22]. The polar angles β_1 and β_2 are the angles that molecules AB and CD make with the intermolecular axis, while α_2 is the dihedral angle A – CoM_{AB} – CoM_{CD} – C. The molecules are separated by an intermolecular distance r.

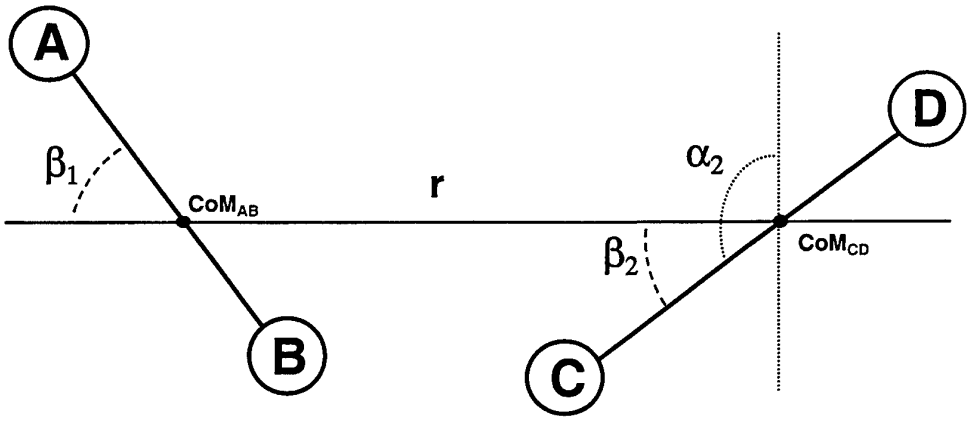

Figure 4: Relative orientation for two axially symmetric molecules AB and CD [22].

3.5 Monte Carlo technique

The Monte Carlo technique allows the calculation of temperature dependent intermolecular potential parameters. The method for two molecules separated by an intermolecular distance r:

1. A large number of calculations (1750 in the cases discussed here) are made over the range of possible relative molecular orientations. values of the internal angles defining the relative intermolecular orientation (for axially symmetric molecules, the three angles β_1 , β_2 and α_2). In practice, this is done by generating random values of β_1 and β_2 from 0 - 180° and α_2 from 0 - 360°.
2. The potential of the system ϕ is calculated for each configuration.
3. The configurations are averaged using summation as an approximation to the integral:

$$\bar{\phi} = -kT \ln\left(\frac{1}{(8\pi^2)^2} \int\int e^{-\phi/kT} d\Omega_1 d\Omega_2 \right)$$

   where Ω_1 and Ω_2 are the orientations of the two molecules.
4. Steps 1 – 3 are repeated for each value of r over a sufficient range to enable a reasonable curve fit of the data around the potential minimum.
5. Temperature dependent parameters ε (maximum well depth of potential), r* (intermolecular distance at maximum well depth) and α (steepness parameter) are obtained by fitting the variation in potential ϕ with intermolecular distance r to the exponential-6 (exp-6) potential:

$$\phi = \frac{\varepsilon}{(\alpha - 6)} \left[6e^{\alpha\left(1-\frac{r}{r^*}\right)} - \alpha\left(\frac{r^*}{r}\right)^6 \right]$$

6. Following Ree [20], the well depth at infinite temperature ε_0 and the temperature dependence of the well depth λ is obtained by fitting ε and T to:

$$\varepsilon = \varepsilon_0 \left(1 + \frac{\lambda}{T} \right)$$

7. Potential curves at different temperatures can be generated by changing the temperature of the calculation. This changes the average potential at each intermolecular distance because of the factor of kT in the integral.

The accuracy of the results obtained using the Monte Carlo method depends primarily on three factors: the number of points obtained, the theoretical method used and the basis set used. Improvements in any of these three factors increases the computation time required. It was found that obtaining 1750 points at each intermolecular distance using a second order Møller-Plesset perturbation method (MP2) with a 6-311^{++}G(d,p) basis set combination gave a satisfactory trade-off between accuracy and computation time for the majority of the systems discussed here (see [18] for a detailed discussion of *ab initio* methods).

3.6 Multipole expansion technique for axially symmetric molecules

For two axially symmetric molecules, approximate values for the spherical part of the potential may be obtained with far fewer calculations than in the Monte Carlo technique. For these two axially symmetric molecules, with orientations as described in Section 3.4, the intermolecular potential can be written:

$$V(r,\beta_1,\beta_2,\alpha_2)=\sum_{l=0}^{\infty}V_{l0}(r,\beta_1,\beta_2,\alpha_2)$$

where

$$V_{l0}(r,\beta_1,\beta_2,\alpha_2)=\sum_{k=0}^{l}f_l^{(l-k,k)}(r)y_l^{(l-k,k)}(\beta_1,\beta_2,\alpha_2)$$

The functions $y_l^{(l-k,k)}(\beta_1,\beta_2,\alpha_2)$, giving the angular dependence of the potential, are multipole expansion functions of angles, in terms of Clebsch-Gordan coefficients and generalised spherical harmonics. For example, the first few terms in the expansion are:

$$\begin{aligned}
V_{00} &= f_0^{(0,0)}(r)\\
V_{10} &= \cos\beta_1 f_1^{(1,0)}(r)-\cos\beta_2 f_1^{(0,1)}(r)\\
V_{20} &= \frac{1}{4}(3\cos 2\beta_1+1)f_2^{(2,0)}(r)+\frac{1}{4}(3\cos 2\beta_2+1)f_2^{(0,2)}(r)\\
&\quad +(\sin\beta_1\sin\beta_2\cos\alpha_2-2\cos\beta_1\cos\beta_2)f_2^{(1,1)}(r)
\end{aligned}$$

The functions $f_l^{(l-k,k)}(r)$ give the radial dependence of the potential. The $f_l^{(l-k,k)}(r)$ reduce at large separations to the usual expansion in terms of the electrostatic spherical tensor multipole moments of molecules **1** and **2**:

$$f_l^{(l-k,k)}(r)\to\frac{4\pi}{\sqrt{2(l-k)+1}\sqrt{2k+1}}\frac{Q_{l-k,0}^{(1)}Q_{k,0}^{(2)}}{r^{l+1}}$$

For axially symmetric molecules, an approximate result may be obtained by solving the set of equations for $f_l^{(l-k,k)}(r)$ up to fixed multipole order. For example, for l=2 (quadrupole), there are six unknown functions:

$$f_0^{(0,0)}(r),\ f_1^{(1,0)}(r),\ f_1^{(0,1)}(r),\ f_2^{(2,0)}(r),\ f_2^{(0,2)}(r),\ f_2^{(1,1)}(r)$$

For l=4 (hexadecapole), this increases to fifteen:

$f_0^{(0,0)}(r)$, $f_1^{(1,0)}(r)$, $f_1^{(0,1)}(r)$, $f_2^{(2,0)}(r)$, $f_2^{(1,1)}(r)$, $f_2^{(0,2)}(r)$,
$f_3^{(3,0)}(r)$, $f_3^{(2,1)}(r)$, $f_3^{(1,2)}(r)$, $f_3^{(0,3)}(r)$, $f_4^{(4,0)}(r)$, $f_4^{(3,1)}(r)$, $f_4^{(2,2)}(r)$, $f_4^{(1,3)}(r)$, $f_4^{(0,4)}(r)$

Hence, if we know $V(r,\beta_1,\beta_2,\alpha_2)$ for six different angular configurations (in the quadrupole case) or fifteen different configurations (in the hexadecapole case) we may solve the set of six (quadrupole) or fifteen (hexadecapole) linear equations for the unknowns (if they are linearly independent). This number reduces if the symmetry of the molecule renders some of the unknowns redundant.

A set of seventeen possible molecular configurations is given in the Appendix, shown for a non-identical pair of axially symmetric molecules. Three linear combinations were used to obtain the spherically symmetric part of the intermolecular potential (V_0), one at the l=2 (quadrupole) level (labelled CB) and two at the l=4 (hexadecapole) level (labelled CAD and CBAD):

$$CB: \quad V_0 = -\frac{1}{12}V(C1)-\frac{1}{12}V(C2)+\frac{1}{2}V(C3)+\frac{1}{6}V(B1)+\frac{1}{6}V(B2)+\frac{1}{6}V(B3)+\frac{1}{6}V(B4)$$

$$CAD: \quad V_0 = \frac{2}{5}V(C1)+\frac{1}{30}V(A1)+\frac{1}{30}V(A4)+\frac{4}{15}V(D1)+\frac{4}{15}V(D4)$$

$$\begin{aligned} CBAD: \quad V_0 = {} & \frac{13}{28}V(C1)+\frac{1}{12}V(C2)-\frac{61}{210}V(C3)+\frac{1}{14}V(B1)+\frac{1}{14}V(B2) \\ & +\frac{1}{14}V(B3)+\frac{1}{14}V(B4)-\frac{4}{105}V(A1)-\frac{4}{105}V(A4)+\frac{2}{15}V(D1) \\ & +\frac{2}{15}V(D4)+\frac{2}{15}V(D2)+\frac{2}{15}V(D5) \end{aligned}$$

If the molecules are identical (eg, HF) several configurations become redundant (ie, the following pairs of configurations are identical: A4 and A1, B4 and B1, B3 and B2, D4 and D1, D5 and D2, and D6 and D3) and the corresponding expression for the spherically symmetric part. If both molecules are identical and both have centres of symmetry (ie, are members of the $D_{\infty h}$ point group, eg, H_2 or CO_2), the set of configurations reduces even further (A1≡A2≡A3≡A4, B1≡B2≡B3≡B4, C1≡C2, D4≡D1, D5≡D2, D6≡D3). Redundancies in configurations for other symmetries (eg, one H_2 molecule and one HF) can be analogously derived.

For the Multipole Expansion technique which involves the gathering of far fewer points compared to the Monte Carlo technique, the method and basis set could be improved in most cases to MP4/6-311^{++}G(3df, 2pd).

4. Results and Discussion

4.1 Hydrogen fluoride (HF)

4.1.1 Monte Carlo technique

The average intermolecular potentials obtained via the Monte Carlo (MC) technique and the exp-6 curve fits for two hydrogen fluoride (HF) molecules at various temperatures are shown in Figure 5. The parameters obtained from the curve fitting are given in Table 2. Also shown for comparison are results from Zerilli and Jones [21] derived from fitting molecular beam spectroscopic data of Barton and Howard [22], labelled ZJBH. As expected, as the temperature increases, the intermolecular potential well depth (ε) decreases, the radius at which the well depth minimum occurs (the intermolecular equilibrium distance, r^*) increases and the steepness parameter (α) also increases. The Monte Carlo curve for 100 000 K (effectively infinite temperature) is very similar to the ZJBH curve at infinite temperature, and the associated parameters (Table 2) are also very similar. The corresponding curve of well depth variation with temperature and the fit of the relationship $\varepsilon = \varepsilon_0 (1+\lambda/T)$ are shown in Figure 6 [6] and the parameters obtained are given in Table 3. It can be seen that the Monte Carlo and the ZJBH results are generally in reasonable agreement.

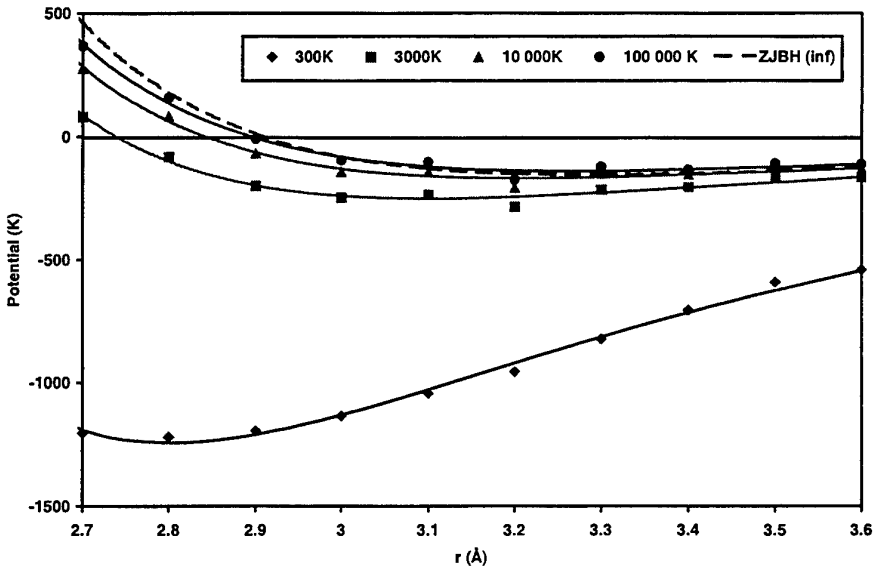

Figure 5: Average intermolecular potential curves with exp-6 fits (2.7-3.6Å) for HF/HF using the Monte Carlo technique (MP2/6-311++G(d,p))

[6] The temperature dependent well depth correction, $\varepsilon = \varepsilon_0 (1+\lambda/T)$, is only valid at high temperature [23], so the deviation of the curves at low temperature is neither surprising nor important in the current context.

Table 2: HF/HF Monte Carlo (MC) results calculated at various temperatures and results of Zerilli and Jones (ZJBH) [21]

T(K)	ε (K)		r* (Å)		α	
	MC[7]	ZJBH [21]	MC[3]	ZJBH [21]	MC[3]	ZJBH [21]
300	1241.9	1389	2.80	2.62	10.96	11.58
2 000	313.3	389	3.04	3.00	12.92	12.24
3 000	249.5	317[8]	3.10	3.06	13.11	12.53
10 000	167.0	202	3.20	3.20	13.43	13.24
100 000 (inf)	138.4	152[9]	3.26	3.28[4]	13.60	13.65[4]

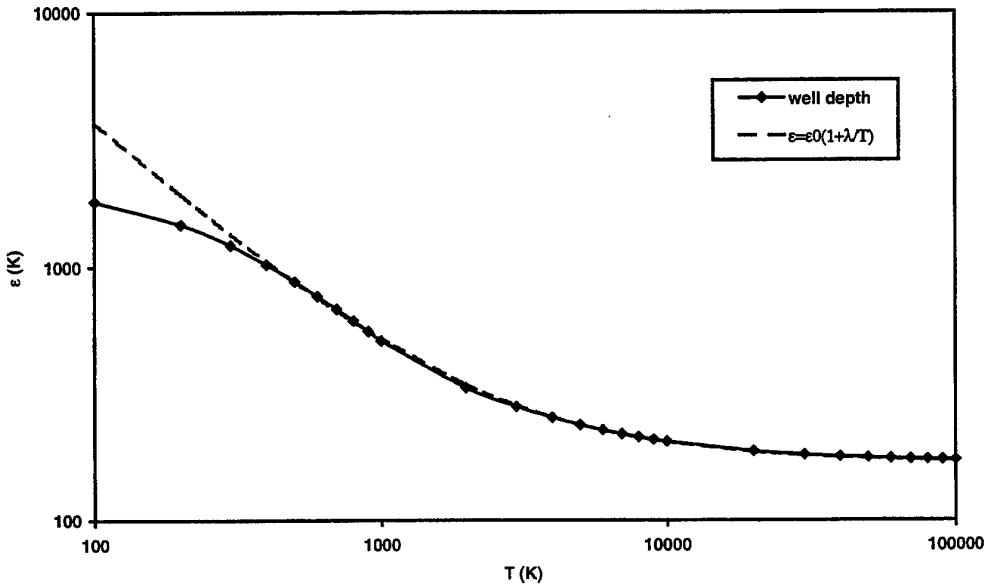

Figure 6: Well depth variation with temperature for HF/HF using the Monte Carlo technique and fit to $\varepsilon = \varepsilon_0 (1+\lambda/T)$ (fit 700 – 100 000 K)

Table 3: Well depth relationship parameters for HF/HF

Source	ε_0 (K)	λ (K)
MC[10]	169	2090
ZJBH [21]	152	3250

[7] exp-6 fit of 2.7 – 3.6 Å Monte Carlo data.
[8] from $\varepsilon=\varepsilon_0(1+\lambda/T)$.
[9] calculated at infinite temperature.
[10] $\varepsilon=\varepsilon_0(1+\lambda/T)$ fit of 700 – 100 000 K.

4.1.2 *Multipole expansion technique*

The intermolecular potential curves obtained for several configurations of the HF/HF system are shown in Figure 7.

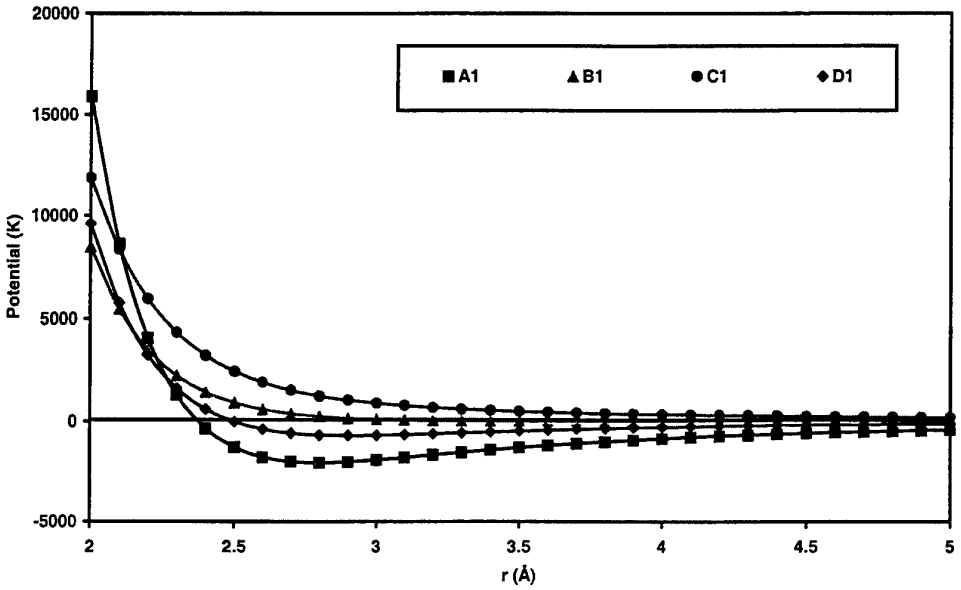

Figure 7: Intermolecular potential curves for HF/HF for several configurations used in the multipole expansion technique (MP4/6-311++G(3df,2pd))

It can be seen that the potentials vary as might be expected by examination of the configurations given in the Appendix. For example, the A1 configuration is one in which the hydrogen fluoride molecules are arranged end-on with the hydrogen of one molecule facing the fluorine of the other (ie, H-F···H-F). Thus, the dipoles of the molecules are aligned and as the molecules are brought towards one another (reducing r), there is a deep potential well at the equilibrium separation distance of about 2.8 Å. The potential rises rapidly as r is reduced further and repulsive forces predominate. On the other hand, in the B1 configuration, the hydrogen fluoride molecules are arranged side-on with the dipoles of each molecule aligned:

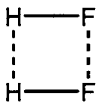

As the molecules are brought closer together, repulsive forces predominate throughout and there is no minimum to the potential energy curve (or, more correctly, the

minimum is zero at r = ∞). The potential curves for the other configurations can be rationalised in a similar manner.

The three average potentials from the multipole expansion technique described in Section 3.6 (labelled ME(CB), ME(CAD) and ME(CBAD)), are shown in Figure 8 for the system of two hydrogen fluoride molecules. For comparison, also shown in Figure 8 are the curve (at effectively infinite temperature, ie 100 000 K) from the Monte Carlo analysis above (labelled MC(inf)) and the curve from the data of Zerilli and Jones [21] calculated at infinite temperature determined from data of Barton and Howard [22] (labelled ZJBH(inf)). The derived parameters are given in Table 4. It can be seen that the averages at the hexadecapole level (ME(CAB) and ME(CBAD)) are much more accurate than that at the quadrupole level (ME(CB)). These higher level averages are close to the ZJBH(inf) values, however, in this case, the Monte Carlo results are much closer.

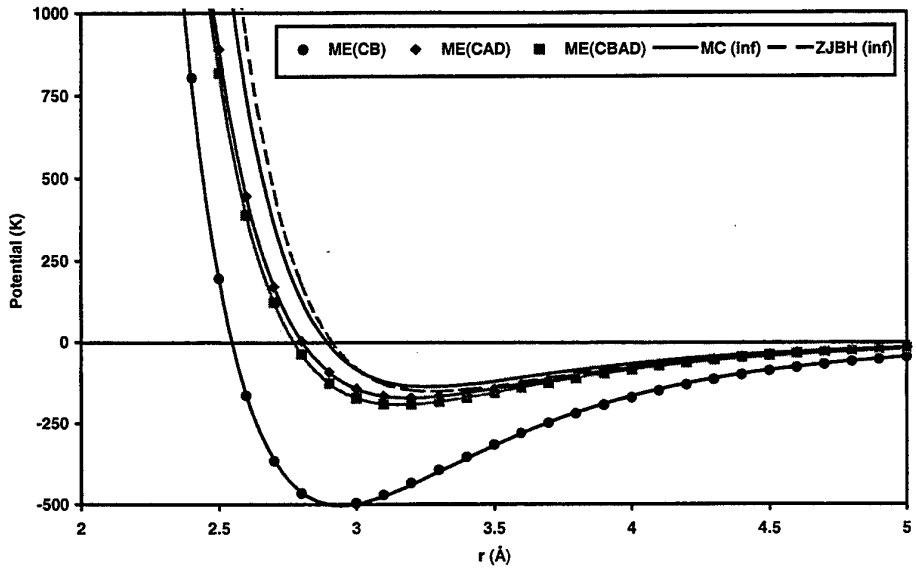

Figure 8: Average intermolecular potential curves for HF/HF using the multipole expansion technique (MP4/6-311++G(3df,2pd))

Table 4: Summary of intermolecular potential parameters for HF/HF

Source	ε_0 (K)	r^* (Å)	α
ME (CB)[11]	504.0	2.94	10.8
ME (CAD)[7]	172.2	3.19	12.3
ME (CBAD)[7]	193.1	3.16	12.1
MC (inf)[12]	138.4	3.26	13.6
ZJBH (inf) [21]	152.0	3.28	13.7

[11] exp-6 fit of 2.5 – 5.0 Å multipole expansion data.

[12] exp-6 fit of 2.7 – 3.6 Å Monte Carlo data at 100 000 K (ie, effectively infinite temperature).

4.2 Hydrogen (H_2)

4.2.1 Monte Carlo technique

Plots of the intermolecular potential at various temperatures using the Monte Carlo technique for the H_2/H_2 system are shown in Figure 9. Note the scale used on the ordinate axis of this graph. It can be seen that there is negligible difference between the potential curves as the temperature increases. For comparison, also shown are results from liquid-state perturbation theory calculations matched to high-pressure data (labelled JZ) [10, 24]. The calculated parameters are given in Table 5.

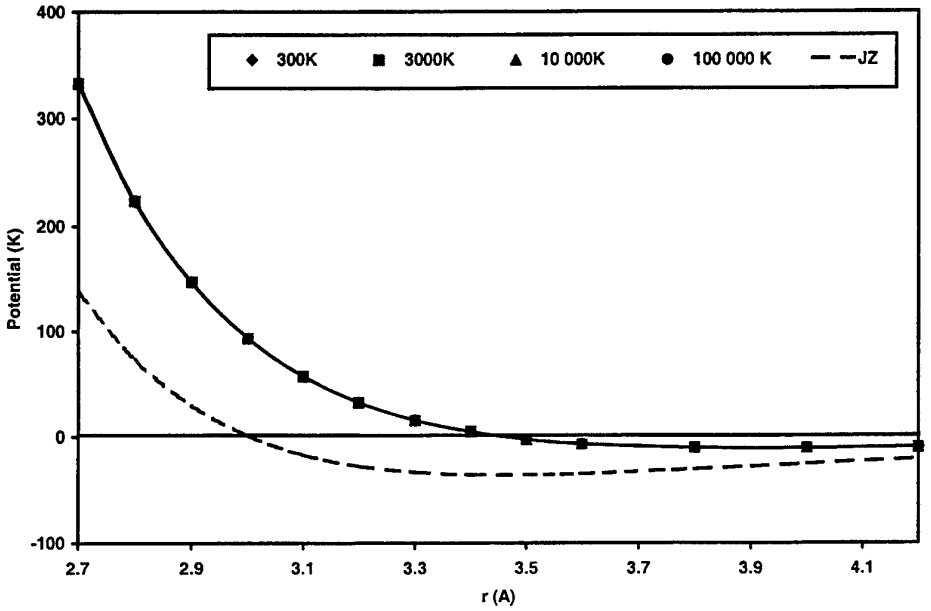

Figure 9: Average intermolecular potential curves with exp-6 fits (2.7-4.2Å) for H_2/H_2 using the Monte Carlo technique (MP2/6-311++G(d,p))

Table 5: H_2/H_2 Monte Carlo (exp-6 fit of 2.7 – 4.2 Å) results calculated at various temperatures and results of Jones and Zerilli (JZ) [10, 24]

T (K)	ε (K)	r^* (Å)	α
300	10.9	3.92	12.9
2 000	10.8	3.92	12.9
3 000	10.8	3.92	12.9
10 000	10.8	3.92	12.9
100 000 (inf)	10.8	3.92	12.9
JZ [10, 24]	36.0	3.46	11.1

The well depth variation with temperature is given in Figure 10. There is negligible change in the well depth over the complete temperature range (noting again the scale

on the ordinate axis and remembering that the ordinate scale in the corresponding figure for the HF/HF system above (Fig. 6) was logarithmic). The parameters obtained for the H_2/H_2 system are given in Table 6. The very small temperature dependence observed in the graph is also reflected in the very small value of λ.

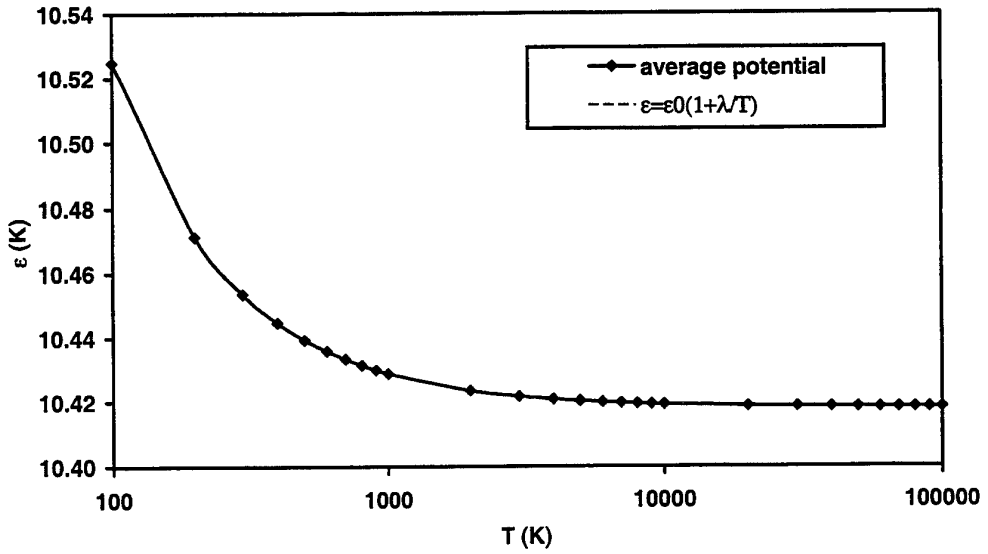

Figure 10: Well depth variation with temperature for H_2/H_2 using the Monte Carlo technique and fit to $\varepsilon = \varepsilon_0 (1+\lambda/T)$ (fit 700 – 100 000 K)

Table 6: Well depth relationship parameters for H_2/H_2

Source	ε_0 (K)	λ (K)
MC[13]	10	1
JZ [10, 24]	36	0

4.2.2 *Multipole expansion technique*

The intermolecular potential curves for H_2/H_2 for some of the configurations from the multipole expansion (ME) technique are shown in Figure 11. The same curves are shown in Figure 12 with the ordinate scale expanded to better illustrate the angular dependence of the potential. It can be seen that the angular dependence is much less significant for the H_2/H_2 system than previously seen for HF/HF (Fig. 7). This is, of course, to be expected from the fact that HF has a strong dipole moment which is absent in H_2.

[13] $\varepsilon=\varepsilon_0(1+\lambda/T)$ fit of 700 – 100 000 K.

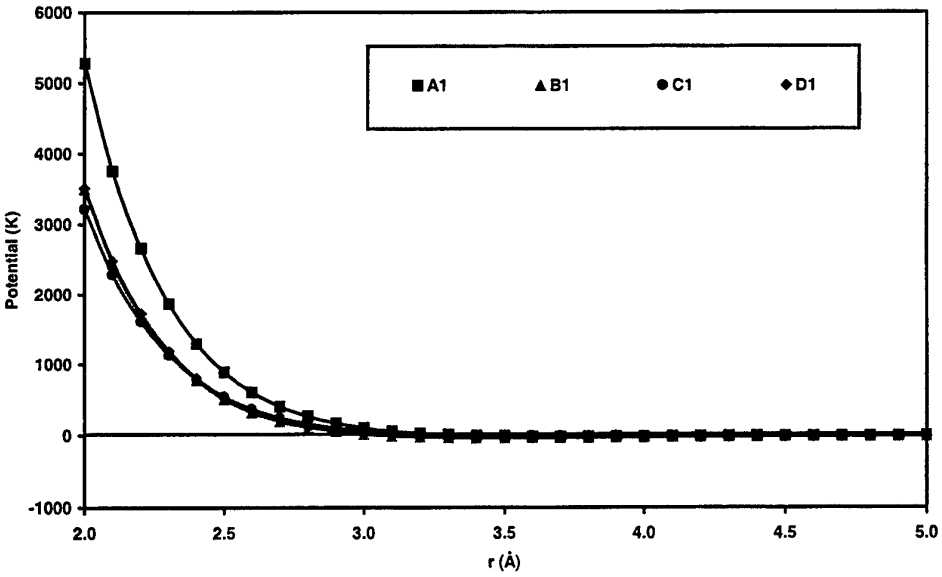

Figure 11: Intermolecular potential curves for H_2/H_2 for several configurations used in the multipole expansion technique (MP4/6-311++G(3df,2pd))

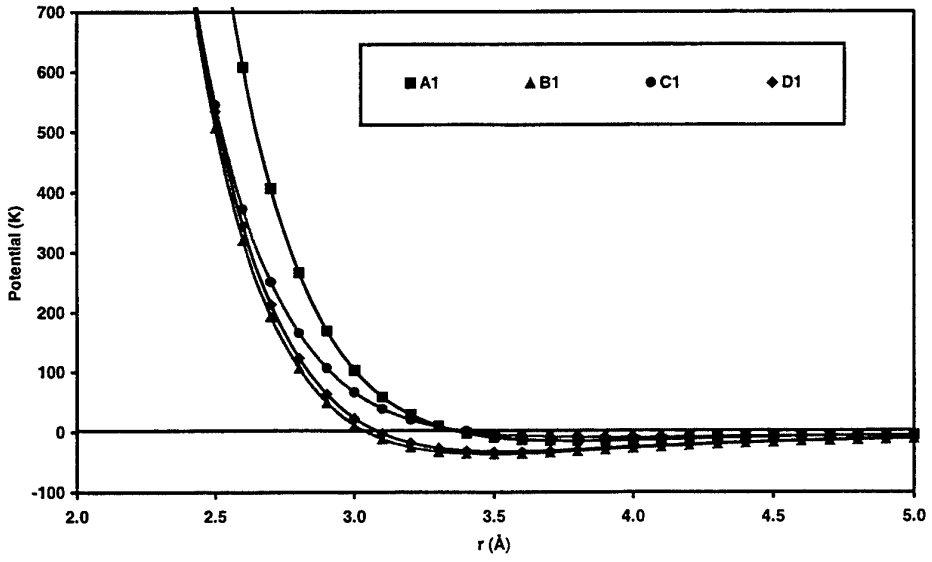

Figure 12: Intermolecular potential curves (expanded ordinate scale) for H_2/H_2 for several configurations used in the multipole expansion technique MP4/6-311++G(3df,2pd))

The plots of average potential are shown in Figure 13 and the parameters obtained are given in Table 7. Again, the corresponding results from the Monte Carlo analysis at 100 000 K (labelled MC (inf)) and results from the data of Jones and Zerilli [10, 24] (labelled JZ) are given for comparison.

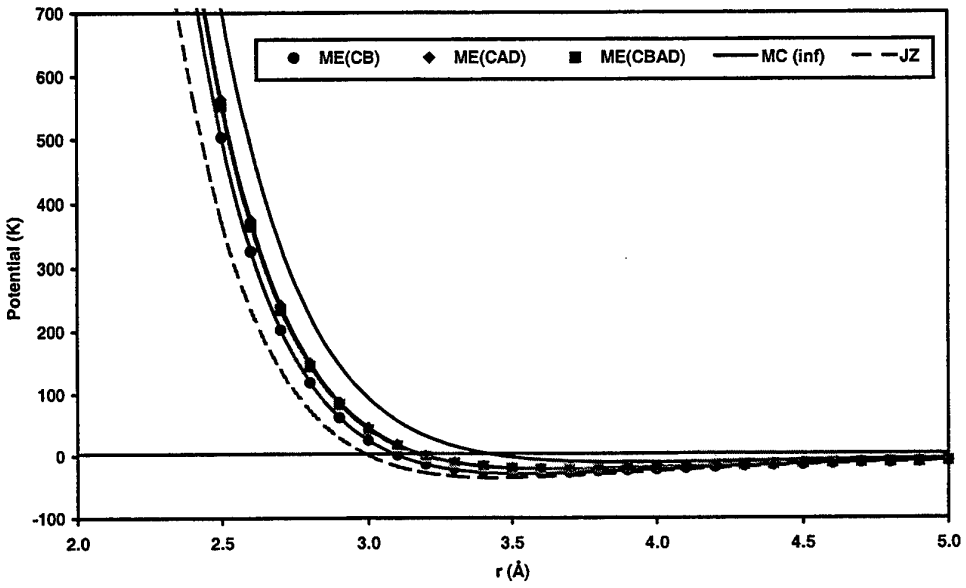

Figure 13: Average intermolecular potential curves for H_2/H_2 using the multipole expansion technique (MP4/6-311++G(3df,2pd))

Table 7: Summary of intermolecular potential parameters for H_2/H_2

Source	ε_0 (K)	r (Å)	α
ME (CB)[14]	29.3	3.55	11.8
ME (CAD)[10]	21.9	3.65	12.1
ME (CBAD)[10]	22.5	3.64	12.1
MC (inf)[15]	10.8	3.92	12.9
JZ [10, 24]	36.0	3.46	11.1

It can be seen that the results at the hexadecapole level (CAD and CBAD) are very close to one another. In this case, the Multipole Expansion results are closer than the Monte Carlo results to those of Jones and Zerilli [10, 24] (in fact, the results at the quadrupole level, CB, appear to be closest). However, given the very small values of ε_0, all the results are reasonably close.

[14] fit 2.5 – 5.0 Å.

[15] exp-6 fit of 2.7 – 4.2 Å Monte Carlo data at 100 000 K (ie, effectively infinite temperature).

4.3 Nitrogen (N_2)

4.3.1 Monte Carlo technique

Plots of the intermolecular potential for the N_2/N_2 system at various temperatures are shown in Figure 14 along with the curve from the data of Jones and Zerilli [10, 24]. The corresponding parameters are given in Table 8. It can be seen that the attractive parts of the potential curves are all similar (ie, not dependent on temperature) and that the minima (well depths) of the potential curves are all similar. This is also reflected in the plot of well depth against temperature (Fig. 15) and in the calculated well depth relationship parameters given in Table 9.

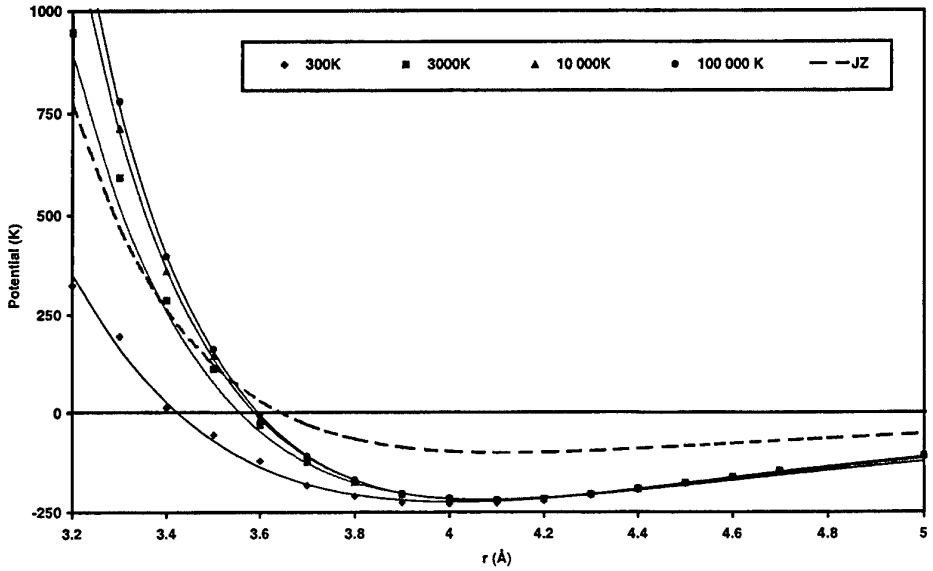

Figure 14: Average intermolecular potential curves with exp-6 fits (3.4-4.7Å) for N_2/N_2 using the Monte Carlo technique (MP2/6-311++G(d,p))

Table 8: N_2/N_2 Monte Carlo (exp-6 fit of 3.4 – 4.7 Å) results calculated at various temperatures and results of Jones and Zerilli (JZ) [10, 24]

T (K)	ε (K)	r^* (Å)	α
300	223.7	4.01	9.9
2 000	217.7	4.08	11.6
3 000	217.9	4.08	11.9
10 000	218.8	4.08	12.6
100 000 (inf)	219.4	4.08	12.9
JZ [10, 24]	100.0	4.12	13.3

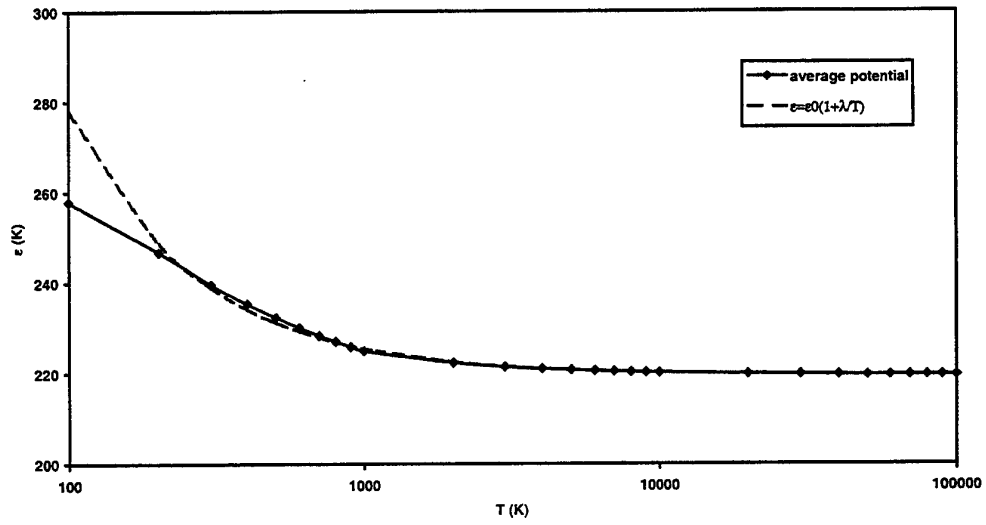

Figure 15: Well depth variation with temperature for N_2/N_2 using the Monte Carlo technique and fit to $\varepsilon = \varepsilon_0 (1+\lambda/T)$ (fit 700 – 100 000 K)

Table 9: Well depth relationship parameters for N_2/N_2

Source	ε_0 (K)	λ (K)
MC[16]	220	27
JZ [10]	100	0

4.3.2 *Multipole expansion technique*

The intermolecular potential curves for each configuration are shown in Figure 16 and, with an expanded ordinate scale, in Figure 17. The observed potential curves show a great deal of angular dependence, with the end-on configuration (A1) rising rapidly as the nitrogen atoms are brought closer together. The average potential curves are shown in Figure 18 and the parameters obtained from the curve fitting are given in Table 10.

[16] $\varepsilon = \varepsilon_0 (1+\lambda/T)$ fit of 700 – 100 000 K.

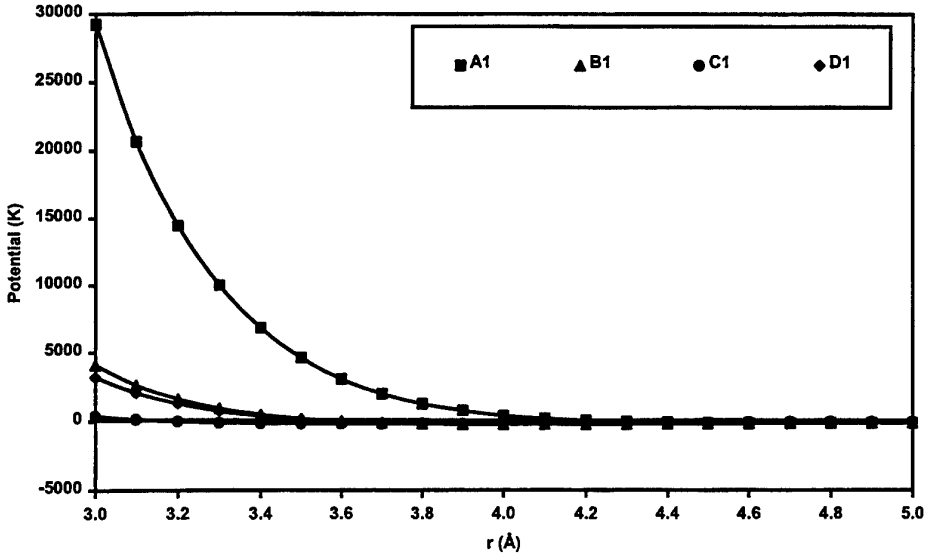

Figure 16: Intermolecular potential curves for N_2/N_2 for several configurations used in the multipole expansion technique (MP4/6-311^{++}G(3df,2pd))

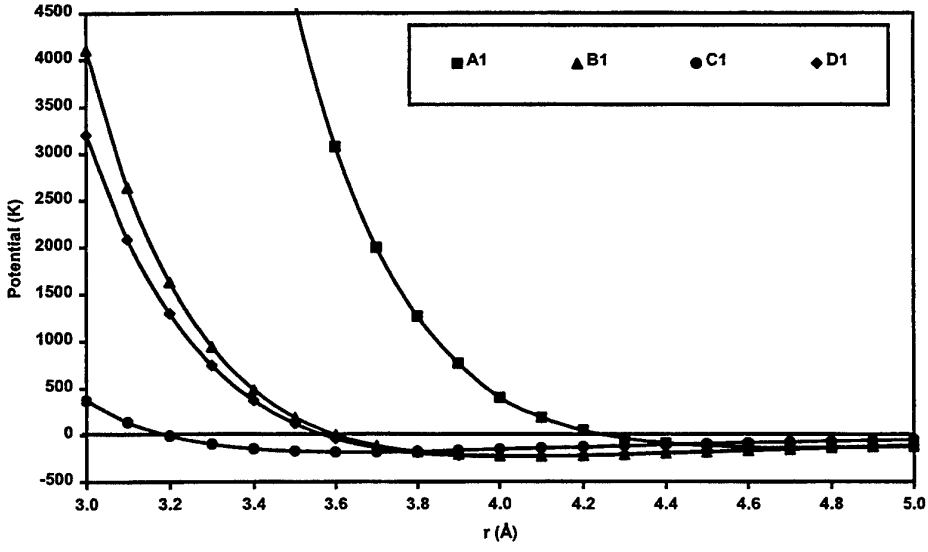

Figure 17: Intermolecular potential curves (expanded ordinate scale) for N_2/N_2 for several configurations used in the multipole expansion technique (MP4/6-311^{++}G(3df,2pd)).

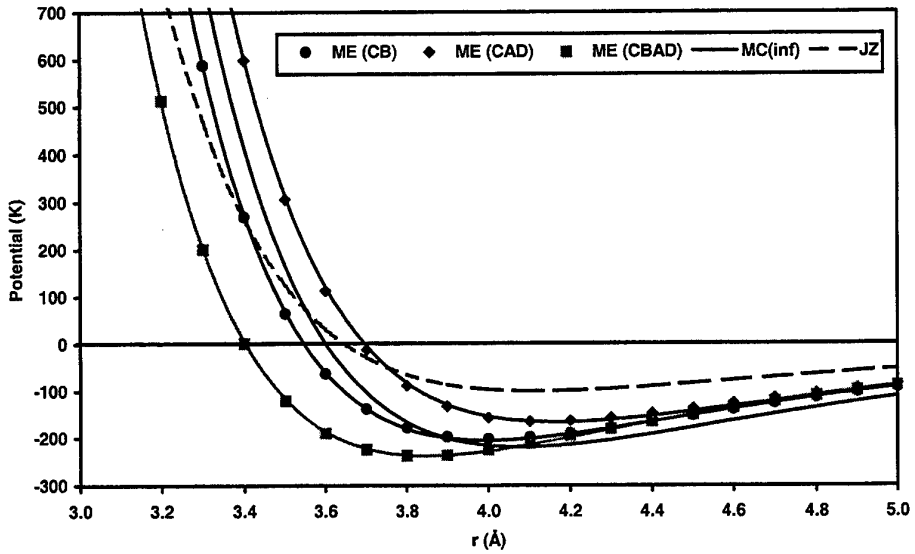

Figure 18: Average intermolecular potential curves for N_2/N_2 using the multipole expansion technique (MP4/6-311++G(3df,2pd)).

Table 10: Summary of intermolecular potential parameters for N_2/N_2

Source	ε_0 (K)	r (Å)	α
ME (CB)[17]	205.4	4.00	13.7
ME (CAD)[13]	166.2	4.17	13.6
ME (CBAD)[13]	238.2	3.85	13.2
MC (inf)[18]	219.4	4.08	12.9
JZ [10, 24]	100.0	4.12	13.3

4.4 Carbon monoxide (CO)

4.4.1 Monte Carlo technique

Plots of the intermolecular potential for the CO/CO system at various temperatures are shown in Figure 19 along with the curve from the data of Jones and Zerilli [10, 24]. The corresponding parameters are given in Table 11. It can be seen that the attractive parts of the potential curves at large intermolecular distances and the minima (well depths) of the potential curves are all similar (ie, not dependent on temperature). This is also reflected in the plot of well depth against temperature (Fig. 20) and in the calculated well depth relationship parameters given in Table 12.

[17] fit 3.0 – 5.0 Å.

[18] exp-6 fit of 3.4 – 4.7 Å Monte Carlo data at 100 000 K (ie, effectively infinite temperature).

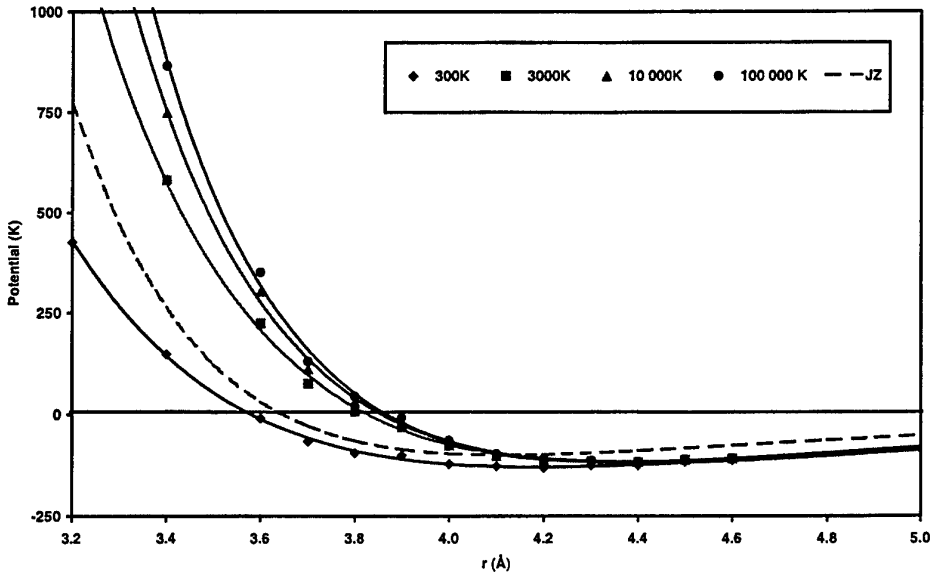

Figure 19: Average intermolecular potential curves with exp-6 fits (3.2-4.6Å) for CO/CO using the Monte Carlo technique (MP2/6-311++G(d,p))

Table 11: CO/CO Monte Carlo (exp-6 fit of 3.2 – 4.6 Å) results calculated at various temperatures and results of Jones and Zerilli (JZ) [10, 24]

T (K)	ε (K)	r* (Å)	α
300	129.5	4.19	10.0
2 000	120.6	4.39	11.0
3 000	120.0	4.39	11.4
10 000	118.2	4.39	12.4
100 000 (inf)	116.4	4.37	13.3
JZ [10, 24]	100.0	4.12	13.3

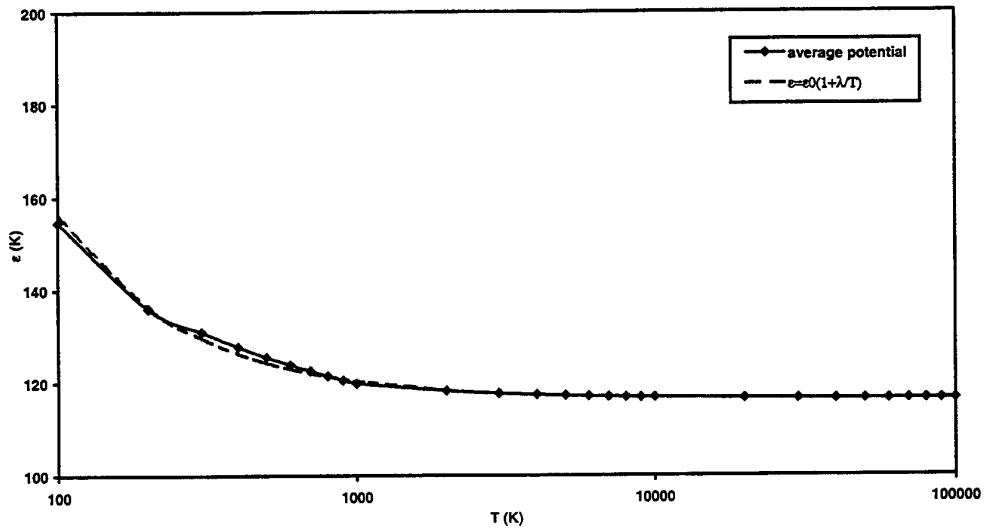

Figure 20: Well depth variation with temperature for CO/CO using the Monte Carlo technique and fit to $\varepsilon = \varepsilon_0 (1+\lambda/T)$ (fit 700 – 100 000 K)

Table 12: Well depth relationship parameters for CO/CO

Source	ε_0 (K)	λ (K)
MC[19]	116	34
JZ [10]	100	0

4.4.2 *Multipole expansion technique*

The intermolecular potential curves for each configuration are shown in Figure 21, and with an increased ordinate scale in Figure 22. As in the case of N_2, there is a great deal of angular dependence of the potential however, whereas in the N_2/N_2 case (Figs. 16 and 17) the curve for the B1 configuration rises rapidly in a similar manner to the curve for the D1 configuration, in the CO/CO case, the B1 curve rises much slower, ie, the repulsion is lower at similar intermolecular distances. This is probably due to the dipole present in CO, which gives a δ+ charge to the carbon and a δ- charge to the oxygen in each molecule. Then, due to the different atomic masses of the carbon and oxygen atoms, the centre of mass of each molecule is closer to the oxygen than the carbon. Consequently, in the B1 configuration (Fig. 23), the carbon of one CO molecule is close to the oxygen of the other molecule, giving rise to an electrostatic attraction which counteracts the repulsion from the non-bonding overlap of the electron clouds.

[19] $\varepsilon = \varepsilon_0 (1+\lambda/T)$ fit of 700 – 100 000 K.

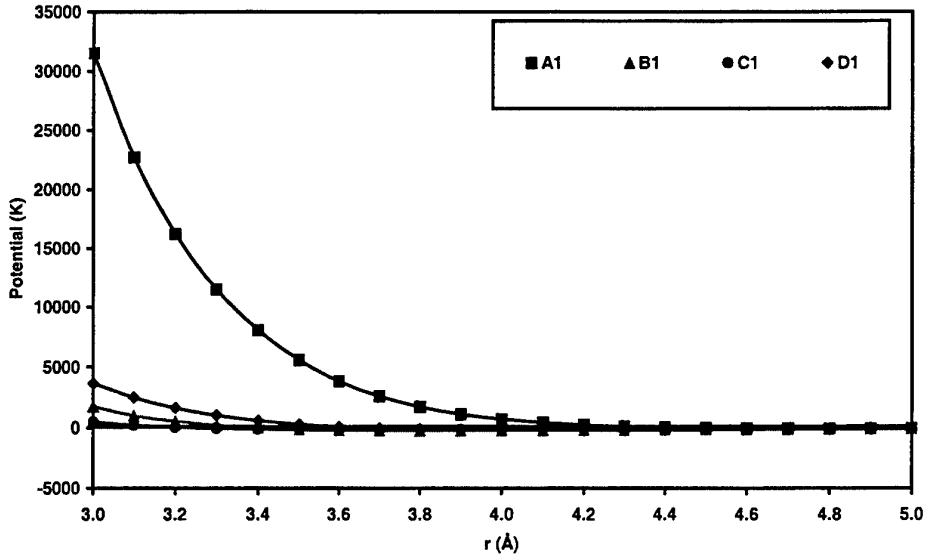

Figure 21: Intermolecular potential curves for CO/CO for several configurations used in the multipole expansion technique (MP4/6-311++G(3df,2pd))

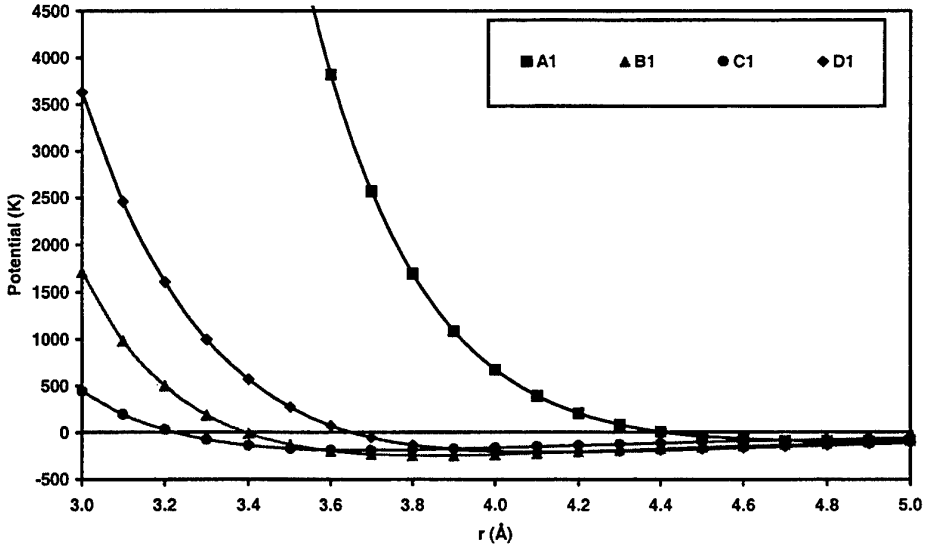

Figure 22: Intermolecular potential curves (expanded ordinate scale) for CO/CO for several configurations used in the multipole expansion technique (MP4/6-311++G(3df,2pd)).

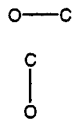

Figure 23: B1 configuration for CO/CO.

The average potential curves are shown in Figure 24 and the parameters obtained from the curve fitting are given in Table 13. As might be expected, the results are very similar to those for the N_2/N_2 system.

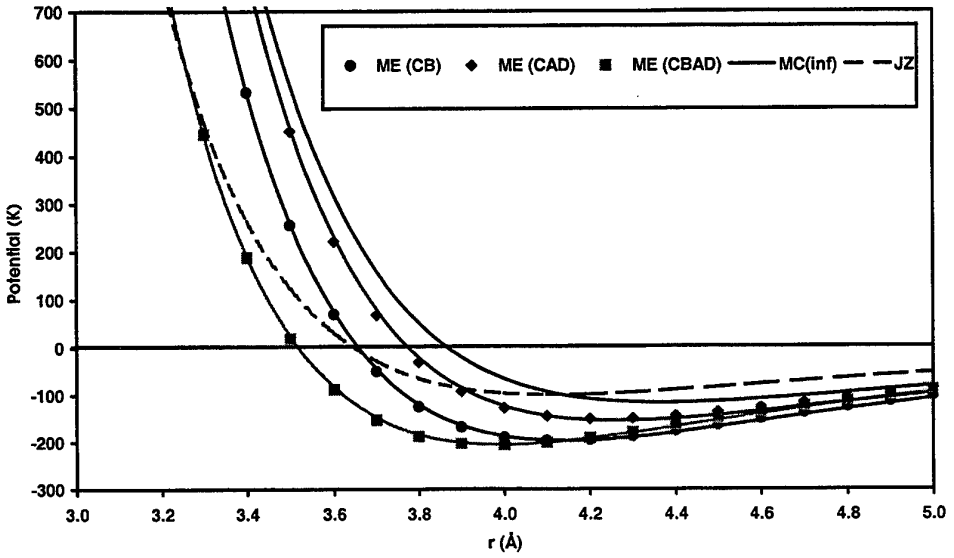

Figure 24: Average intermolecular potential curves for CO/CO using the multipole expansion technique (MP4/6-311++G(3df,2pd)).

Table 13: Summary of intermolecular potential parameters for CO/CO

Source	ε_0 (K)	r (Å)	α
ME (CB)[20]	197.1	4.14	13.0
ME (CAD)[16]	154.7	4.27	13.3
ME (CBAD)[16]	205.0	3.99	12.7
MC (inf)[21]	116.4	4.37	13.3
JZ [10, 24]	100.0	4.12	13.3

[20] fit 3.0 – 5.0 Å.

[21] exp-6 fit of 3.2 – 4.6 Å Monte Carlo data at 100 000 K (ie, effectively infinite temperature).

4.5 Carbon dioxide (CO_2)

4.5.1 Monte Carlo technique

Plots of the intermolecular potential for the CO_2/CO_2 system at various temperatures are shown in Figure 25 along with the curve from the data of Jones and Zerilli [10, 24]. The corresponding parameters are given in Table 14. Again, it can be seen that the attractive parts of the potential curves are all similar (ie, not dependent on temperature) and that the minima (well depths) of the potential curves are all similar. This is also reflected in the plot of well depth against temperature (Fig. 26) and in the calculated well depth relationship parameters given in Table 15.

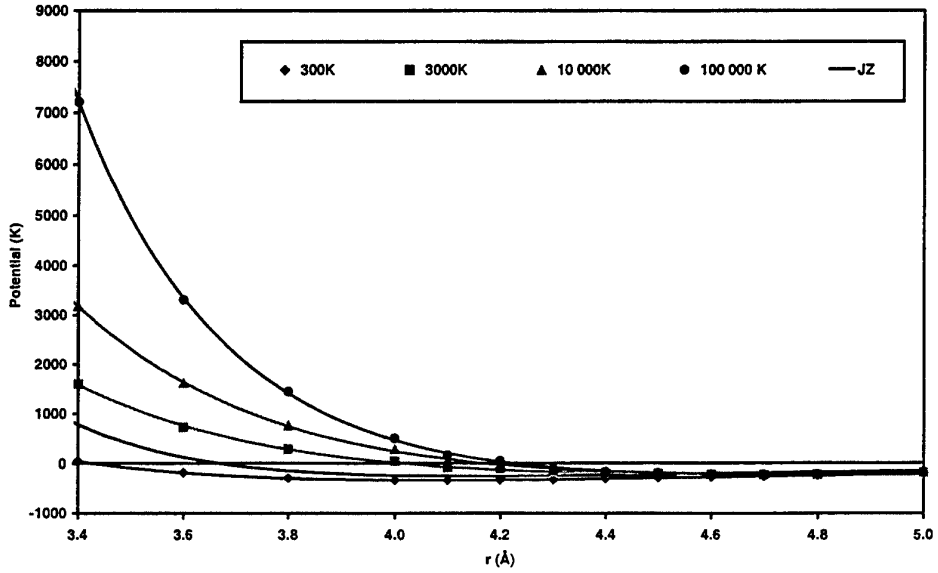

Figure 25: Average intermolecular potential curves with exp-6 fits (3.4 –5.0 Å) for CO_2/CO_2 using the Monte Carlo technique (MP2/6-311++G(d,p))

Table 14: CO_2/CO_2 Monte Carlo (exp-6 fit of 3.4 – 5.0 Å) results calculated at various temperatures and results of Jones and Zerilli (JZ) [10, 24]

T (K)	ε (K)	r^* (Å)	α
300	329.0	4.07	9.4
2 000	210.9	4.57	10.4
3 000	206.4	4.66	10.6
10 000	216.4	4.80	11.5
100 000 (inf)	212.5	4.73	15.1
JZ [10, 24]	250.0	4.15	13.4

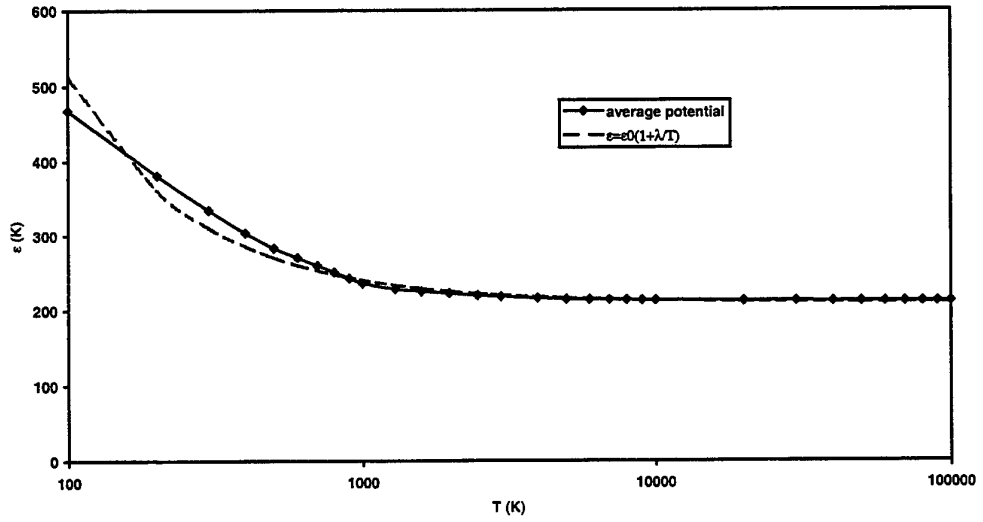

Figure 26: Well depth variation with temperature for CO_2/CO_2 using the Monte Carlo technique and fit to $\varepsilon = \varepsilon_0 (1+\lambda/T)$ (fit 700 – 100 000 K)

Table 15: Well depth relationship parameters for CO_2/CO_2

Source	ε_0 (K)	λ (K)
MC[22]	210	144
JZ [10]	250	0

4.5.2 *Multipole expansion technique*

Attempts were made to obtain EOS parameters for CO_2 using the multipole expansion technique. Studies at the MP4/6-311^{++}G(3df,2pd) level proved intractable on our computers so the studies were conducted at the MP2/6-311^{++}G(3df,2pd) level. The potential curves obtained from these studies for each configuration are shown in Figure 27. The same data shown in a plot with an expanded ordinate scale are shown in Figure 28. It can be seen that there is a significant amount of bonding interaction occurring at intermolecular distances of around 3.5 Å in the A1 (end-on) configuration. This is not surprising, as for two CO_2 molecules, when the intermolecular distance (distance between the carbon atoms on the two different molecules) is 3.5Å, the distance between the two closest oxygen atoms is comparable to the C-O bond length (1.167Å). Consequently, expressions for the spherically symmetric potential containing contributions from the A configurations (ie, CAD and CBAD) are probably unreliable.

[22] $\varepsilon = \varepsilon_0 (1+\lambda/T)$ fit of 700 – 100 000 K.

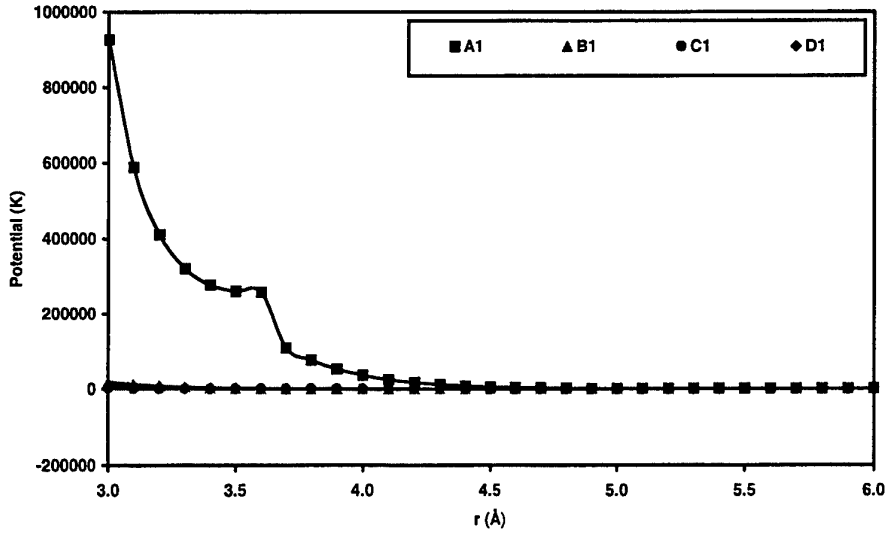

Figure 27: Intermolecular potential curves for CO_2/CO_2 for several configurations used in the multipole expansion technique (MP2/6-311++G(3df,2pd)). A bonding interaction is apparent in the curve for the A1 configuration at about 3.5 Å.

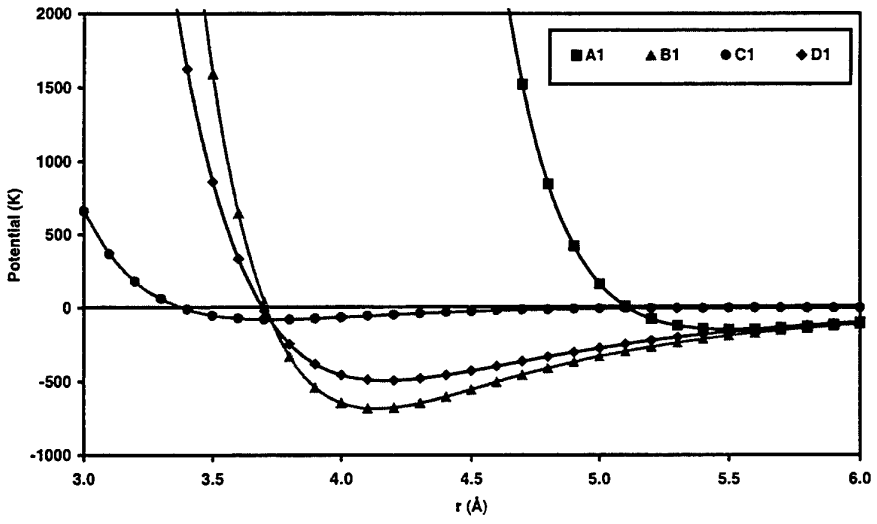

Figure 28: Intermolecular potential curves (increased ordinate scale) for CO_2/CO_2 for several configurations used in the multipole expansion technique (MP2/6-311++G(3df,2pd)).

The curves from the three averaging expressions are shown in Figure 29 and the results are given in Table 16. Again, the results for CAD are probably unreliable and are given for information only. A meaningful curve fit could not even be obtained for ME (CBAD). The results for CB should be reliable, however as seen before, results from this second order multipole expansion are generally not as accurate as those using a fourth order expansion.

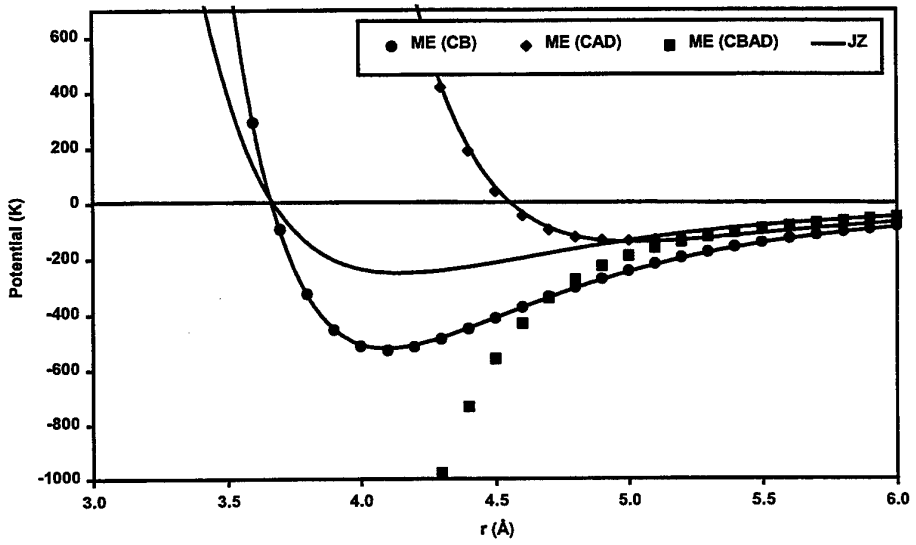

Figure 29: Average intermolecular potential curves for CO_2/CO_2 using the multipole expansion technique (MP2/6-311++G(3df,2pd)). ME (CAD) and ME (CBAD) data are probably unreliable due to bonding interactions in the A1 (end-on) configuration

Table 16: Summary of intermolecular potential parameters for CO_2/CO_2

Source	ε_0 (K)	r (Å)	α
ME (CB)[23]	519.9	4.10	15.3
ME (CAD)[24]	139.8	5.02	18.4
ME (CBAD)	n/a	n/a	n/a
MC (inf)[25]	212.5	4.73	15.1
JZ [10, 24]	250.0	4.15	13.4

[23] fit 3.5 – 6.0 Å.

[24] fit 3.8 – 6.0 Å. ME (CAD) results probably unreliable due to bonding interactions as discussed in text.

[25] exp-6 fit of 3.4 – 5.0 Å Monte Carlo data at 100 000 K (ie, effectively infinite temperature).

5. Example – Shock Hugoniot for Liquid Nitrogen

The shock Hugoniot for liquid nitrogen was calculated using the parameters from the multipole expansion technique given in Table 10. The results compared with experimental data given by Dick [25] are shown in Figures 30 and 31. It can be seen that the calculated curves are a very good match to the experimental data.

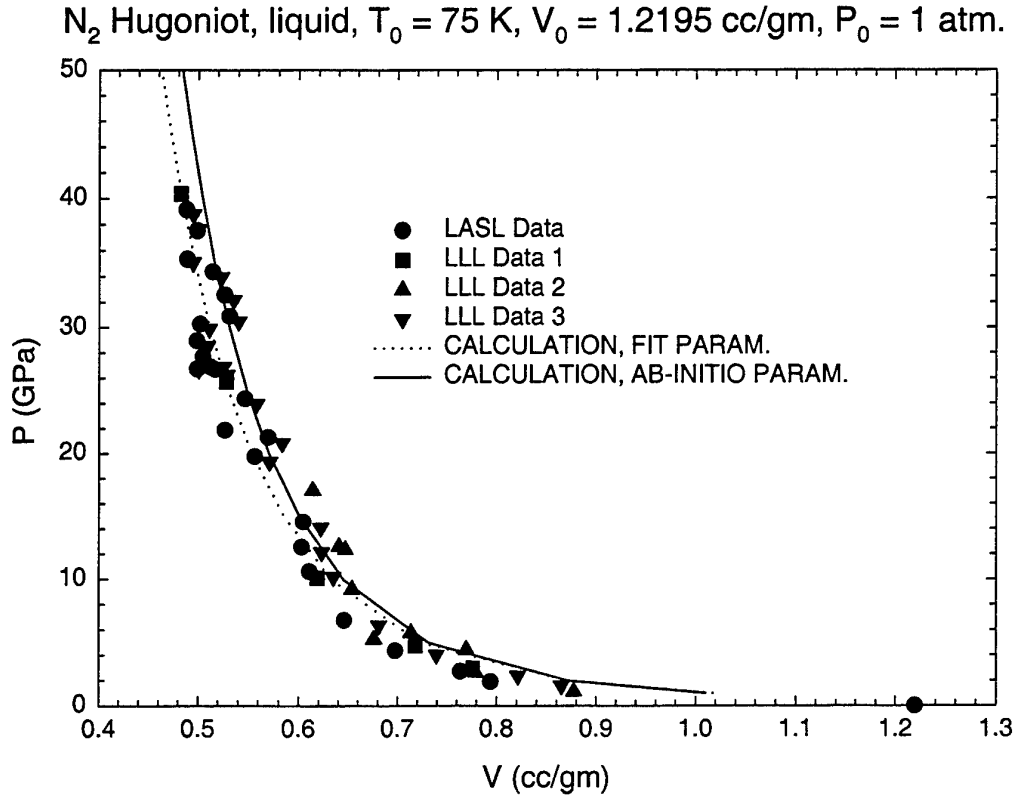

Figure 30: Shock Hugoniot for liquid nitrogen (pressure vs specific volume)

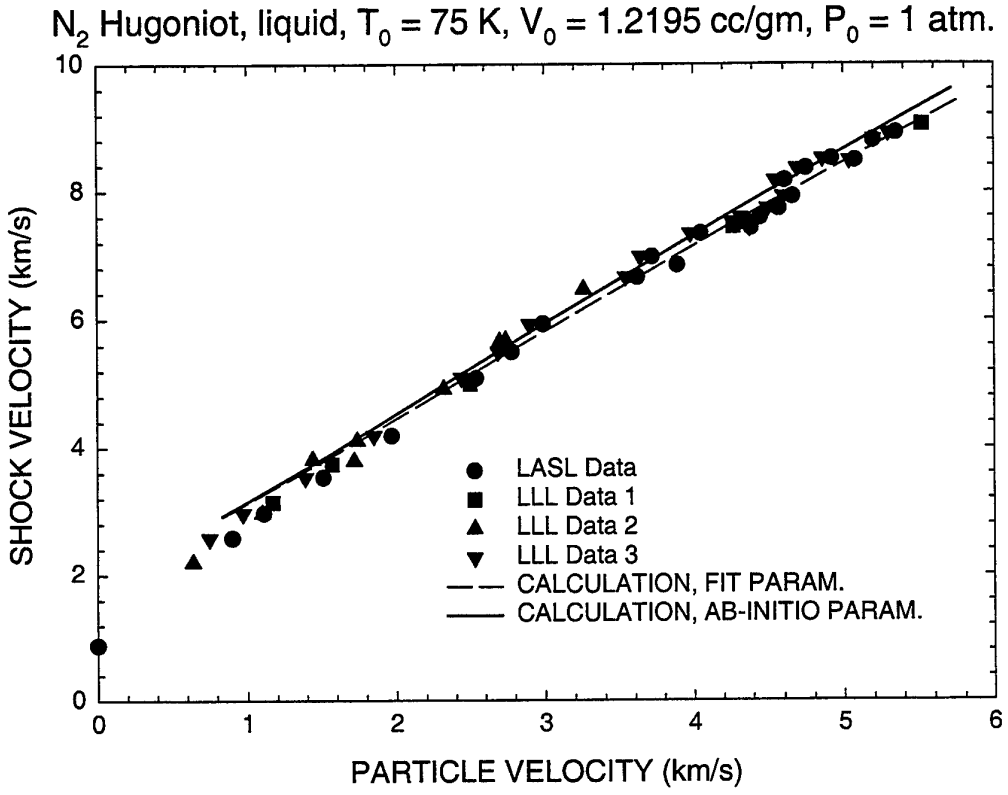

Figure 31: Shock velocity vs specific volume for liquid nitrogen

6. Conclusions and Further Work

This document describes two methods for *ab initio* calculation of intermolecular potential parameters for use in equations of state based on the formalism of Week, Chandler and Andersen [11] which describes fluids whose molecules interact via a spherically symmetric, modified Buckingham (exp-6) potential. The two methods described are:

- a Multipole Expansion method, suitable for analytical calculation of intermolecular potential parameters for axially symmetric molecules
- a Monte Carlo method, which can be used to obtain average potential energy parameters for any molecules within the accuracy of the *ab initio* method used.

The results obtained are in reasonable agreement with those obtained from fitting experimental results [10, 24]. It remains now to use these parameters in calculations of explosive performance parameters. Preliminary results for the fluorine-containing explosive FEFO (bis(2-fluoro-2,2-dinitroethyl)formal) appear promising [26].

The systems under study here constitute intermolecular potentials for pairs of axially symmetric identical molecules. For mixed molecules (eg, HF/H_2), the Lorentz-Berthelot mixing rule is often invoked to estimate the intermolecular potential from the potentials of the pairs of identical molecules. The methods described here afford a method of directly measuring these heteromolecular potentials and, consequently, of checking the validity of the parameters used in the Lorentz-Berthelot rule. This aspect will be addressed in a forthcoming publication [6]. The application of the Monte Carlo method to non-axially symmetric molecules, in particular H_2O, will also be described in a subsequent publication [2].

7. References

1. Mader, C.L., Numerical modeling of explosives and propellants, 2nd ed, CRC Press, Boca Raton, Fl, USA (1998).

2. White, A., *Ab initio* calculation of intermolecular potential parameters for H_2O, DSTO Technical Note (in publication).

3. Fickett, W. and Davis, W.C., Detonation, University of California Press (1979).

4. Cooper, P.W., Explosives Engineering, Wiley-VCH (1997).

5. Fickett, W., Introduction to detonation theory, University of California Press (1985).

6. White, A., *Ab initio* calculations of heteromolecular intermolecular potentials and the Lorentz-Berthelot mixing rule, DSTO Technical Note (in publication).

7. eg, see Atkins, P.W., Physical Chemistry, Oxford University Press (1978).

8. Ref [1] referring to: (a) Kistiakowsky, G.B. and Wilson, E.B., The hydrodynamic theory of detonation and shock waves, US Office of Scientific Research and Development Report OSRD-114 (1941). (b) Kistiakowsky, G.B. and Wilson, E.B., Report on the prediction of detonation velocities of solid explosives, US Office of Scientific Research and Development Report OSRD-69 (1941). (c) Becker, R., Eine zustandsgleichung für stickstoff bei grossen dichten, Zeitschrift für Physik, **4**, 393 (1921). (d) Becker, R., Physikalisches über feste und gasformige sprengstoffe, Zeitschrift für Technische Physik, **3**, 249 (1922).

9. Cowan, R.D. and Fickett, W., Calculation of the detonation products of solid explosives with the Kistiakowsky-Wilson equation of state, J. Chem. Phys., **24**, 932 (1956).

10. Jones, H.D. and Zerilli, F.J., Theoretical equation of state for aluminized nitromethane, J. Appl. Phys., **69**, 3893 (1991).

11. Weeks, J.D., Chandler, D. and Andersen, H.C., Role of repulsive forces in determining the equilibrium structure of simple liquids, J. Chem. Phys., **54**, 5237 (1971).

12. Lennard-Jones, J.E., The determination of molecular fields. I. From the variation of the viscosity of a gas with temperature, Proc. Roy. Soc. (Lond.) **106A**, 441 (1924).

13. Lennard-Jones, J.E., The determination of molecular fields. II. From the equation of state of a gas, Proc. Roy. Soc. (Lond.) **106A**, 463 (1924).

14. Rapaport, D.C., The art of molecular dynamics simulation, Cambridge University Press, Cambridge, UK (1995).

15. Ross, M. and Ree, F.H., Repulsive forces of simple molecules and mixtures at high density and temperature, J. Chem. Phys., **73**, 6146 (1980).

16. Ree, F.H., A statistical mechanical theory of chemically reacting multiphase mixtures: Application to the detonation properties of PETN, J. Chem. Phys., **81**, 1251 (1984).

17. Gaussian 98, Revision A.3, M.J. Frisch, G.W. Trucks, H.B. Schlegel, G.E. Scuseria, M.A. Robb, J.R. Cheeseman, V.G. Zakrzewski, J.A. Montgomery, Jr., R.E. Stratmann, J.C. Burant, S. Dapprich, J.M. Millam, A.D. Daniels, K.N. Kudin,

M.C. Strain, O. Farkas, J. Tomasi, V. Barone, M. Cossi, R. Cammi, B. Mennucci, C. Pomelli, C. Adamo, S. Clifford, J. Ochterski, G.A. Petersson, P.Y. Ayala, Q. Cui, K. Morokuma, D.K. Malick, A.D. Rabuck, K. Raghavachari, J.B. Foresman, J. Cioslowski, J.V. Ortiz, B.B. Stefanov, G. Liu, A. Liashenko, P. Piskorz, I. Komaromi, R. Gomperts, R.L. Martin, D.J. Fox, T. Keith, M.A. Al-Laham, C.Y. Peng, A. Nanayakkara, C. Gonzalez, M. Challacombe, P.M.W. Gill, B. Johnson, W. Chen, M.W. Wong, J.L. Andres, C. Gonzalez, M. Head-Gordon, E.S. Replogle, and J.A. Pople, Gaussian, Inc., Pittsburgh PA, 1998.

18. Dorsett, H. and White, A., Overview of molecular modelling and *ab initio* molecular orbital methods suitable for use with energetic materials, DSTO General Document (in publication).

19. Møller, C. and Plesset, M.S., Notes on an approximation treatment for many-electron systems, Phys. Rev., **46**, 618 (1934).

20. Ree, F.H., Equilibrium properties of high-density fluids, J. Chem. Phys., **64**, 4601 (1976).

21. Zerilli, F.J. and Jones, H.D., High pressure equation of state for HF, CF_4 and F_2, in High Pressure Science and Technology-1993, AIP Conference Proceedings 309, American Institute of Physics, New York, 113 (1994).

22. Barton, A.E. and Howard, B.J., An intermolecular potential-energy surface for $(HF)_2$, Faraday Discuss. Chem. Soc., **73**, 45-62 (1982).

23. Ree, F.H., Viecelli, J.A. and van Thiel, M., Equation of state of insensitive high explosives, 11th International Detonation Symposium (1998).

24. Jones, H.D. and Zerilli, F.J., Multipole effects on the equation of state for reaction products of explosives, 10th International Detonation Symposium, 449 (1995).

25. Dick, R.D., Shock wave compression of benzene, carbon disulfide, carbon tetrachloride, and liquid nitrogen, J. Chem. Phys., **52**, 6021 (1970).

26. White, A., Zerilli, F.J. and Jones, H.D., An *ab initio* method for estimating equation of state parameters, APS Conference on Shock Compression of Condensed Matter, Snowbird, Ut, USA (27th June – 2nd July 1999).

Appendix A: Angular Configurations for Multipole Expansion Technique

A1 (0, 0, 0)

A2 (0, 180, 0)

A3 (180, 0, 0)

A4 (180, 180, 0)

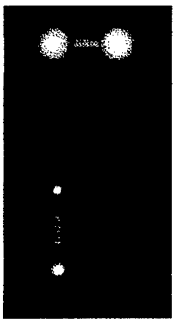

B1 (0, 90, 0)

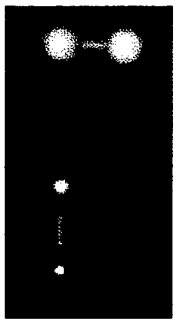

B2 (180, 90, 0)

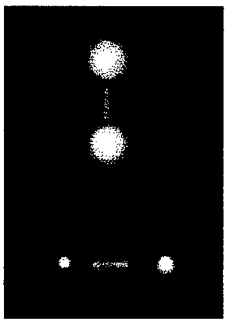

B3 (90, 0, 0)

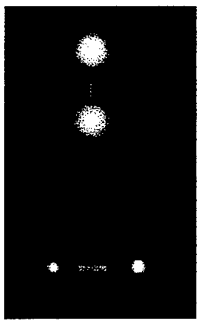

B4 (90,180,0)

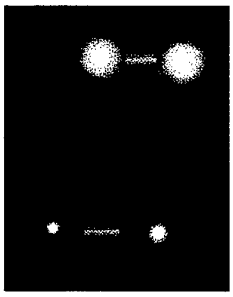

C1 (90,90,0)

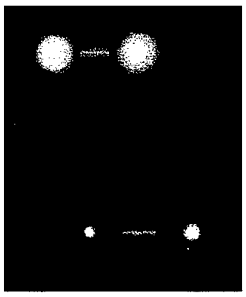

C2 (90,90,180)

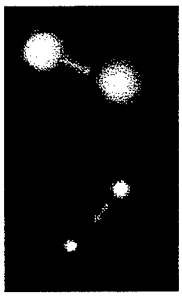

C3 (90,90,90)

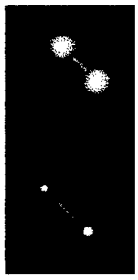

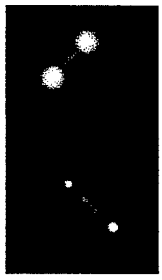

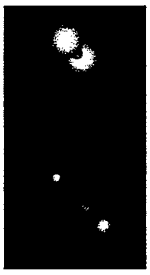

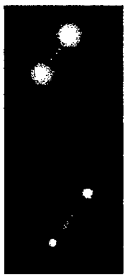

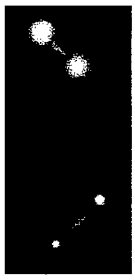

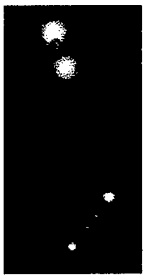

D1 (45,45,0) D2 (45,45,180) D3 (45,45,90) D4 (135,135,0) D5 (135,135,180) D6 (135,135,90)

DISTRIBUTION LIST

Ab Initio Calculation of Intermolecular Potential Parameters for Gaseous Decomposition Products of Energetic Materials

A. White, F.J. Zerilli and H.D. Jones

AUSTRALIA

DEFENCE ORGANISATION

Task Sponsor

President – Australian Ordnance Council

S&T Program

Chief Defence Scientist
FAS Science Policy
AS Science Corporate Management
} shared copy

Director General Science Policy Development
Counsellor Defence Science, London (Doc Data Sheet)
Counsellor Defence Science, Washington (Doc Data Sheet)
Scientific Adviser to MRDC Thailand (Doc Data Sheet)
Scientific Adviser Policy and Command
Navy Scientific Adviser
Scientific Adviser - Army
Air Force Scientific Adviser
Director Trials

Aeronautical and Maritime Research Laboratory

Director
Chief of Weapons Systems Division
Research Leader Joint and Intelligence
Head Propulsion Systems Technology
Head Explosives
Head Pyrotechnics
Dr C. Doolan (WSD)
Dr H. Dorsett (WSD)
Dr D.A. Jones (MPD)
Dr J.P. Lu (WSD)
Task Manager/Author(s):
Dr A. White (10 copies for distribution between authors)

DSTO Library and Archives

Library Fishermans Bend (Doc Data sheet only)
Library Maribyrnong (Doc Data sheet only)
Library Salisbury (1 copy)
Australian Archives
Library, MOD, Pyrmont (Doc Data sheet only)
*US Defense Technical Information Center, 2 copies
*UK Defence Research Information Centre, 2 copies
*Canada Defence Scientific Information Service, 1 copy
*NZ Defence Information Centre, 1 copy

National Library of Australia, 1 copy

Capability Development Division
Director General Maritime Development (Doc Data Sheet only)
Director General Land Development (Doc Data Sheet only)
Director General C3I Development (Doc Data Sheet only)
Director General Aerospace Development (Doc Data Sheet only)

Navy
SO (Science), Director of Naval Warfare, Maritime Headquarters Annex, Garden Island, NSW 2000. (Doc Data Sheet only)

Army
ABCA Standardisation Officer, Puckapunyal, (4 copies)
SO (Science), DJFHQ(L), MILPO Enoggera, Queensland 4051 (Doc Data Sheet)
NAPOC QWG Engineer NBCD c/- DENGRS-A, HQ Engineer Centre Liverpool Military Area, NSW 2174 (Doc Data Sheet only)

Intelligence Program
DGSTA Defence Intelligence Organisation
Manager, Information Centre, Defence Intelligence Organisation

Corporate Support Program
OIC TRS, Defence Regional Library, Canberra

UNIVERSITIES AND COLLEGES
Australian Defence Force Academy
Library
Head of Aerospace and Mechanical Engineering
Dr Kenneth R. Harris, School of Chemistry
Senior Librarian, Hargrave Library, Monash University (Doc Data Sheet only)
Librarian, Flinders University

OTHER ORGANISATIONS
NASA (Canberra)
AusInfo

OUTSIDE AUSTRALIA

ABSTRACTING AND INFORMATION ORGANISATIONS
Library, Chemical Abstracts Reference Service
Engineering Societies Library, US
Materials Information, Cambridge Scientific Abstracts, US
Documents Librarian, The Center for Research Libraries, US

INFORMATION EXCHANGE AGREEMENT PARTNERS
Acquisitions Unit, Science Reference and Information Service, UK
Library - Exchange Desk, National Institute of Standards and Technology, US

SPARES (5 copies)
Total number of copies: 61

DEFENCE SCIENCE AND TECHNOLOGY ORGANISATION DOCUMENT CONTROL DATA					1. PRIVACY MARKING/CAVEAT (OF DOCUMENT)
2. TITLE *Ab Initio* Calculation of Intermolecular Potential Parameters for Gaseous Decomposition Products of Energetic Materials					3. SECURITY CLASSIFICATION (FOR UNCLASSIFIED REPORTS THAT ARE LIMITED RELEASE USE (L) NEXT TO DOCUMENT CLASSIFICATION) Document (U) Title (U) Abstract (U)
4. AUTHOR(S) A. White, F.J. Zerilli and H.D. Jones					5. CORPORATE AUTHOR Aeronautical and Maritime Research Laboratory PO Box 4331 Melbourne Vic 3001 Australia
6a. DSTO NUMBER DSTO-TR-1016	6b. AR NUMBER AR-011-531		6c. TYPE OF REPORT Technical Report		7. DOCUMENT DATE August 2000
8. FILE NUMBER J9505/19/33	9. TASK NUMBER JNT00/020	10. TASK SPONSOR PAOC	11. NO. OF PAGES 43	12. NO. OF REFERENCES 26	
13. URL ON WORLD WIDE WEB http://www.dsto.defence.gov.au/corporate/reports/DSTO-TR-1016.pdf			14. RELEASE AUTHORITY Chief, Weapons Systems Division		
15. SECONDARY RELEASE STATEMENT OF THIS DOCUMENT *Approved for public release* OVERSEAS ENQUIRIES OUTSIDE STATED LIMITATIONS SHOULD BE REFERRED THROUGH DOCUMENT EXCHANGE, PO BOX 1500, SALISBURY, SA 5108					
16. DELIBERATE ANNOUNCEMENT No Limitations					
17. CASUAL ANNOUNCEMENT Yes					
18. DEFTEST DESCRIPTORS Energetic materials, decomposition, intermolecular forces, combustion products, gases					
19. ABSTRACT This document describes the results obtained using two methods for *ab initio* calculation of intermolecular potential parameters for gaseous decomposition products of energetic materials: a Multipole Expansion method, suitable for axially symmetric molecules, and a Monte Carlo method, which can be used to obtain temperature dependent average potential energy parameters for any molecule.					